A Technique for Large Scale Drought Monitoring

(China National 94.8 Technique Import Project)

Z. Su
Y. Yang
J. Zhang
G. Lu
G. Zhou
G.J. Roerink
J. Qi
J. Liu
L. Wang
J. Wen
L. Jia
W. Zheng
Z. Yue
X. Chen

Alterra-rapport 683

Alterra, Green World Research, Wageningen, 2003

Contents

Preface

Drought is a natural reoccurring phenomenon in a region during which the land ecosystem suffers from insufficient water supply and can be thought as a periodic climatic phenomenon. Drought is directly caused by less rainfall during a long period such that the supply of water resources can not satisfy the need of land ecosystem.

Drought is one of the main natural disasters that human being has suffered since the ancient era. Even in nowadays with well developed science and technology, drought is still the most serious natural disaster that affects agriculture production and human lives. The frequently occurred droughts and desertification events have become the major worldwide environmental and climatic problems in recent year. With the rapid increase of the global population and the economic development, the shortage of water resources has become the most serious problem in the new millennium. Such shortage will directly enlarge the areas already threatened by droughts and enhance the drought severity, and consequently the continuous development of social economy and the existence of human living environment will be threatened.

Since the most part of continental China is located in the monsoon climatic zone, where the seasonal and yearly variations of the precipitation are notorious and the spatial and temporal distributions inhomogeneous, large-scale drought disasters frequently occur over the continental China. From historical records, 1056 drought events occurred in the 2155 years from 206 BC to 1949, with one major drought in every two years. The situation is getting even worse since 1949, with the drought affected area reaching about 300 million MU (15 MU = 1 hectare) every year, the grain yield loss caused by the drought is about 10 billion JIN (2 JIN = 1 Kilogram). Especially since the 1990s, nationwide droughts occur year after year, causing more and more grain yield losses. Drought disaster has become a key factor constraining the sustainable development of social economy. According to the forecast, the Chinese population will increase to 1.6 billion by the end of 2040. With this increase of population, shortage of water resources, droughts and food security will become the most concerned issues. Therefore, researches in droughts and development of methodologies for large-scale drought disaster monitoring and early warning in order to reduce the damages caused by drought become important and significant both in theoretical development and practical applications.

According to the practical requirements for drought mitigation, the Water Resources Information Center of the Ministry of Water Resources of China (WRIC/MWR) has developed a hydrological and meteorological drought monitoring operational system in 1996 based on a river basin hydrological model. In this system the potential evaporation and soil water content are derived with a hydrological model using inputs from in-situ meteorological measurements and precipitation. The derived soil water deficit is defined as a drought severity index and is used for the nationwide drought severity assessment and monitoring. This system automatically operates on the basis of the real-time precipitation and meteorological database and produces

daily nationwide soil water deficit, and has been used to advise the drought mitigation in China for many years. However it is felt that there are problems in two aspects that need to be improved: (1) The spatial resolution of derived product is low; the soil water content is derived from only 590 rain-gauge observation sites, thus its regional representativeness is very poor and it is very difficult to extract the soil water deficit at the desired site in time. (2) The hydrological model used in this system is a singe-point model, so that the nationwide soil water deficit is derived by interpolation between the point calculation, and can not reveal the actual spatial situation of soil water deficit realistically in time.

In recent years, Wageningen University and Research Center, Alterra Green World Research in the Netherlands (WUR/Alterra) has achieved notable advances in the applications of satellite remote sensing and has successfully developed a technique on the estimation of drought characteristic parameters, including the land surface albedo, leaf area index, land surface temperature, sensible heat flux, latent heat flux, evaporative fraction and soil wetness. They have also conducted many excellent researches on atmospheric correction of satellite remote sensing data and development of remote sensing image processing software, as well as on microwave soil moisture retrieval. Therefore, both WRIC/MWR and WUR/Alterra have done large amount of work and are mutually complementary on the research and cooperation in large-scale drought monitoring.

In order to import this advanced drought monitoring technique and apply for the nationwide drought monitoring, a project was funded in June 2000 by the National 94.8 Foundation of the Ministry of Water Resources of China. The main goal of this project is to study and import the advanced technique of WUR/Alterra to retrieve the land surface parameters and process the satellite remote sensing images and to improve the ongoing drought monitoring system at WRIC/MWR with the imported technique for providing more directly, more objectively, more completely and more precisely nationwide drought information services.

The project is divided into three phases detailed as following:

First phase (June 2000 to April 2001):
Objective: the design and preparation of the relevant technique for the entire system. The main results are

(1) The data preparation and collection of two years' NOAA/AVHRR, Geostationary Meteorological Satellite data, in-situ precipitation and evaporation etc. data.
(2) The first technical team (four persons) visited WUR/Alterra for one week to understand the theory on drought monitoring and remote sensing image processing and outlined the project technique design; a system structure diagram and data flowchart for the project were drawn and the implementation plan for the technique import and the master working plan were developed.
(3) WUR/Alterra expert visited WRIC/MWR and gave the relevant lectures and technical instructions; the detailed technique and outline of the project were further discussed and addressed.

Second phase (May 2001 to November 2001):

Objective: The transplantation and modification of the technique and software package, the main results are

(1) The second technical team (four persons) visited WUR/Alterra for five weeks to modify SEBS 8.0 (Surface Energy Balance System, version 8.0) from the local application to nationwide application and adaptation for automatic operation requirements. The computational cost became more economic after the modification to original source code.

(2) According the requirements of SEBS and the practical situations in China, an image preprocessing program has been produced for preprocessing the raw NOAA/AVHRR data received in China.

(3) Sensitivity analyses: As the process of SEBS operation is very complicated, involving many parameters and requiring long CPU time, high computational capacity is desired. To increase the computational efficiency, the parameterizations for the several parameters with little effects on the final results have been simplified through sensitivity analysis.

(4) Importation of the ENVI software package to establish the SEBS operational environment. A WUR/Alterra expert visited WRIC/MWR and gave instructions in November 2001. An algorithm for processing the meteorology data has been developed during this visit. Both sides installed and transplanted the SEBS software package at WRIC/MWR.

Third phase (December 2001 to April 2002):

Objective: This phase is aimed at the analysis of final computational results, the improvement of methodology and the feasibility of practical operation. Transplantation of the Harmonic ANalysis of Time Series (HANTS) software package and the compilation of the final report.

(1) The third technical team (5 persons) visited WUR/Alterra for four weeks to finish computation for two-month's data; the preliminary computational results have been analyzed.

(2) WUR/Alterra and WRIC/MWR discussed and addressed how to improve the methodology based on the final computational results.

(3) WUR/Alterra and WRIC/MWR discussed and outlined the final project report and finished the compilation of the technical report by the end of April 2002.

This technique import project has got strong supports from WRIC/MWRC, HUC and WUR/Alterra during its operational period. The project team would like to express sincere thanks to all the supports.

1 Introduction

1.1 Drought disaster in China

Drought is a complex natural disaster, the definition of which depends largely upon practical applications. In general drought is caused by rainfall shortage when rainfall is lower than the climatic mean value. The impacts of rainfall shortage depend upon the meteorological conditions, ecosystem types and social economical environments. The drought disaster are currently defined or generally recognized as following five categories:

(1) Meteorological drought identified according to the local precipitation, which is defined when the local precipitation is lower than the climatic mean. It is also expressed with the combination of air temperature and rainfall abnormality sometimes.
(2) Agricultural drought identified according to the soil water content and crop water requirement. When the local rainfall and soil water content can not supply sufficient water to the plant during its key developing period, the growth of the plant will then be affected and its production reduced.
(3) Hydrological drought identified according to runoff and groundwater, which is defined with one or more hydrological factors, such as runoff, water storage and groundwater level.
(4) Social economical drought identified according to the water resources requirement and supply. It's defined with water supply anomaly or the gap between the available and the expected supply and can be derived from social or economical indices.
(5) Climatic drought identified according to land surface water and energy balance.

The most region of continental China is located in the monsoon climate zone, where the precipitation is inhomogeneous in temporal and spatial distribution. The annual rainfall events are concentrated in 2-3 months in the monsoon season, and make up more than 70% of the annual precipitation. Especially in the northern China area, 80-90% of annual precipitation may be accumulated in one or a few large rainfall events, while the other period suffers long time drought. China is a country with less rainfall when compared to other countries in the world. The average rainfall per capita in China is only 5006 m^3, while the global average is 33975 m^3, such that China only makes 15% of the world average rainfall per capita. From the availability of water resources, China has only 2300 m^3 water resources per capita, about one-fourth of the world average and is ranked in 109th position allover the world. The available water resources is only 1900 m^3 per MU in land, also only one-fourth of the world average. In addition, due to the rapid social economical development of urbanization, the requirement for water resources increases continuously.

On the other hand, the regional distribution of the average available water resource per capita differs hugely from region to region. For example, it is only about 500m^3

per capita in northern China where the economy is well developed and population density is very high. The water resources availability per hectare is even less amounting to only 6750m^3/hectare in this region. In the northwestern China, the average water resource is relatively high per capita and per hectare because of the smaller population, but the density of water resources is very sparse, causing difficulties to the development and utilization of water resources. Therefore, China is not only a country where drought disasters are potentially very frequent, but it is also a country that suffers easily from drought disasters.

The most serious droughts almost occurred every two years since 1949, with the average affected area reaching about 3.0321×10^8 MU, accounting about 59.3% of the area affected by climatic disasters. The most seriously affected area makes up more than 5.0×10^8 MU in 1956, 1960, 1961 and 1978, with direct grain loss of above 1.0×10^{10} kg. Among all natural disasters, drought disasters have the biggest impacts to the agriculture production. At present, the shortage of water resource is about 30 billion m^3 in the irrigated agricultural area, the grain loss caused by drought disasters amounts 10-15 billion Kg annually. Since the 1990s, the area affected by droughts increases to 24 million Km^2, and is 1.5 times larger than that in the 1950s, and the entire drought affected area enlarges 3 times. In the first four year of the 1990s, the grain loss caused by droughts reaches 35 billion Kg every year. Currently 65 million people and 60 million livestock are still suffering from the shortage of drink water.

In 2001 the area affected by drought disasters was the largest in the whole Chinese history. Most area in China suffers from continuous drought in this year, the drought affected area is more than 0.35 billion MU, among which 0.33 billion MU is dry land, 0.02 billion MU is irrigated land. The drought affected area were distributed in northeastern China, in the Huanghe river and Huaihe river basins and in southwestern China, and is the third year in a row with drought disasters. The main reasons are: The water storage in the reservoir of northern China was too low because of the serious drought in the year before; the precipitation was less than that in the normal years; the water storage in May 2001 was 20% less compared to the last years; The strong wind and spring sandstorm occurred in the northwestern region that accelerated the evaporation and enhanced the drought severity furthermore.

The drought disasters have the following characteristics in China:

(1) Large in area and inhomogeneous in regional distribution

It is reported that 27% of the irrigated land is affected by flooding and drought disasters every year all over the country, among which 60% of them are drought affected area, which indicates that drought affected area is very large. Drought occurs all over the country but it is inhomogeneous in regional distribution. The Huang-Huai-Hai rivers region makes up 50% of the whole drought affected area. The middle and upper parts of Yangtse river basin are also frequently affected by droughts. These two regions make up 60% of the whole drought affected area in China.

(2) High occurrence and long duration

China's large territory is characterised by complicated topography and its climate is mainly controlled by monsoon. Local and regional droughts occur almost every year. For example, the northern, northeastern and southern China suffered from droughts for 8 years in the 13 years from 1979 to 1991. In addition, droughts lasted for two years to the south of the Yangtse river, for two years across the whole country and for one year in the whole Yangtse river basin. In northern China during 1951-1980, large regional droughts prevailed for 12 years, medium droughts lasted for 11 years, and local droughts occurred in 7 years. In the same period, the Yangtse river basin suffered from twenty-eight years droughts of different degrees.

In temporal scale, the drought disasters may occur during the spring-summer, summer-autumn or even spring-summer-autumn periods all over the country. For example, drought disasters usually last for one to two months or four to five months in the northern China. The duration can be even longer in some years. Such as in 1957, 1965, 1968, 1972 and 1986, the droughts lasted for five to seven months. Hot-summer droughts usually occur in the Yangtse river basin, but some regions within the river basin have also suffered continuous long-duration droughts. Such as in 1998, hot-summer drought occurred in the Yangtse river basin, but in the provinces Hunan, Hubei, Shanghai, Jiangsu, Anhui and Guizhou continuous droughts occurred lasting longer than 40 days and even 50-70 days in some regions. In June-August 1994, the Jianghui region has suffered serious hot-summer droughts. The droughts in Anhui, Jiangsu, Hubei provinces lasted for 40-50 days and even reaching two months in some areas. In the same year, spring droughts also occurred in many areas, and the autumn droughts covered even more areas distributed to the south of Yangtse river, in south and north China and in the east part of the northeast region.

(3) Drought accompanied often by simultaneous high temperatures

During many drought disasters, high temperature often occurs simultaneously, which in turn enhances the drought severity. Such situations are most obvious in the Yangtse river basin. Such as the summer drought occurred in June-August 1985, the air temperature was very high during this period with daily average temperature higher than 30 °C. The extreme temperature reached 38 - 40 °C in northeast, southeast of Hubei and in the Three Gorges region. The air temperature was higher than 38°C in Chongqing in the drought period. The air temperature reaches 40-41°C in Fulin and Wanxian cities. For seven days, the air temperature reached 35-37 °C in Hangzhou city. High air temperature accelerated the evaporation and enhanced the drought severity. Serious droughts occurred in May-October 1965 in northern China, when the average air temperature was 1-2 °C higher than that in a normal year, the days with high air temperature ($\geq$ 35°C) counted 10-35 days and were 5-18 days longer than that in a normal year. In the example mentioned previously, when droughts occurred in the Jiang-huai basins in 1994, high air temperature also occurred with 20-40 days of high temperature ($\geq$35 °C).

1.2 Drought monitoring technique and its development

The traditional drought monitoring method is based on the soil water content measured with the gravimetric method or with a neutron probe. The sampling efficiency of these methods are very low, costing a lot of manpower and finance; the regional representativeness of the ground measured data is very poor and difficult for large scale applications. For many years, scientists have explored and arrived other more efficient methods for monitoring drought. In 1965, Palmer gave a definition for drought which meant a continuous and abnormal water deficit (Palmer, 1965). Starting from this idea and based on water balance taking consideration of evapotranspiration, runoff and soil water content, a drought severity index could be defined from hydrological computation and statistics, this is the so-called Palmer Drought Severity Index (PDSI). PDSI has been widely used to describe the drought-affected area and severity in America for many years and is well-known in the world. Its suitability has been tested in Australian, Canada and South Africa. An (1986) used PDSI to analysis of wet and dry climate and assessment of climatic impacts. Yu (1996) proposed a modified Palmer Drought Severity Index model after tested it at 14 sites in China. The result showed that PDSI could be used as an effective tool to monitor regional drought in China. However, the computation of PDSI is very complicated and many parameters are not easy to acquire. In addition, due to some assumptions and subjectivity exist in model establishment and water balance computation, it is only suited for drought monitoring at regional scale but not for real-time large scale applications.

Researchers from Liaoning Hydrology Survey and Design Institute, Sichuan General Hydrology Station and Shaanxi General Hydrology Station have developed local agricultural drought models. The basic principles of these models have taken into account of the relationship between the long term water requirement and supply for the different type crops. The water deficit is expressed with the soil water balance equation, and the drought severity is assessed with its absolute or relative values of the water deficit. This method is practical but only for local applications, while the required data are not easy to obtain. The China National Meteorological Center distributes quarterly nationwide drought severity classification map based on statistical analysis of precipitation and relationship between precipitation and drought and water-logging. As meteorology drought is not always equivalent to the agricultural drought, in addition to its lower temporal and spatial resolution, its application is very limited.

The Water Resources Information Center, the Ministry of Water Resources of China (WRIC/MWR) developed a drought monitoring operational system based on a hydrological model and meteorological data in 1996. The drought severity is assessed with the water deficit which is derived from this hydrology model, the potential evaporation computed from the meteorological data and the local precipitation. This automatic operational system has been continuously operated till present and has given primary results that prove the feasibility for practical drought monitoring with a hydrological model and meteorological data. However, as there is no satellite data as references and the hydrologic model did not take the variations of land surface

properties into account, the spatial resolution of drought product is very low and very large discrepancies appear between the computed results and the practical situation. As a result, the application value of the system is limited in practical drought decision making.

In recent years, assessment of drought severity using the satellite remote sensing technique is a worldwide hot topic. This is especially so for the meteorological satellite observation that covers a large area with frequent overpasses. The United Nations' Food and Agriculture Organization launched a project in 1997, which focused on drought monitoring and corn yield estimation in Southern Africa. Australia scientists have also used remote sensing technique for monitoring crop area, crop development and soil moisture to assist the assessment of drought affected areas. The Center for Remote Sensing of Shaanxi Meteorological Bureau has used a method for using vegetation index calculated with NOAA/AVHRR visible bands data and soil wetness retrieved with infrared brightness temperature to indirectly assess the drought severity. Both research and application results have shown that data from meteorological satellite are an effective tool to monitor real time drought severity with wide application prospective. However, a satellite sensor receives only reflected or emitted electromagnetic signal from the land surface, which can not directly reflect the actual drought severity. At the same time the existence of clouds also perturb the observation data which must be corrected for.

Currently, development of decision-making systems for large-scale drought monitoring and forecast is one hot research topic. Satellite remote sensing and geographic information systems have been widely used in large-scale data extraction and spatial data management as such are used as effective tools for drought monitoring and forecast. Research results show that the large-scale continuous drought are mainly controlled by the abnormal large-scale climate system, although the local feedback especially the variation of the surface albedo, soil wetness have considerable impacts to the drought occurrence. The state-of-the-art in large-scale drought severity monitoring and forecast is based on the land surface energy balance combined with land surface geo-information derived from satellite remote sensing data and coupled with atmospheric and hydrologic models. The mechanisms of the occurrence and development of drought disasters can then be explored with such method and the relevant drought decision-making system be established for drought mitigation and prevention purposes.

1.3 The goal and content of the imported technique

In order to establish a nationwide large-scale drought severity operational monitoring system, this project will import the technique for the estimation of land surface parameters from the meteorological satellite remote sensing data. This technique has been developed by Dr. Z. Bob Su and colleagues (Su et al., 1998; Su, 2001, 2002) from Wageningen University and Research Centre, Alterra green world research. This technique has significant advantages in fast and economically retrieval of land surface geo-information at large scale and can directly monitor or indirectly retrieve

the inhomogeneous drought parameters at large scale, which can not be achieved by traditional methods. Although soil water content is one of the most important parameters used in drought monitoring and forecast, current soil water models only evaluate the soil water content based on the energy balance equation in which the energy and water distribution at the land-atmosphere interface is simply considered as known parameters inputted into the model. However, since the spatial distributions of the energy and soil water content are difficult to acquire practically, such soil water content models are not applicable for practical applications.

Other types of soil water content models that are based on limited observation network data are not reliable too. Since the land surface heterogeneity has not been sufficiently considered, these models can not evaluate the regional distribution of soil water content for the purpose of monitoring drought severity. As satellite remote sensing can provide the regional distribution of inhomogeneous land surface parameters with consideration of the inhomogeneity of soil water content, the possibility for practical monitoring soil water content at large scale becomes feasible. To this end, Dr. Z. Bob Su and colleagues have developed a quantitative technique for the determination of land surface albedo, leaf area index, thermal infrared radiation flux, land surface temperature, sensible heat flux, latent heat flux, evaporation fraction and soil wetness which can be used to characterize the drought severity. The relevant software and accessories have also been developed, that can be used instantly to estimate the drought severity at large scales.

The current technique is built on the applications for small area and ideal database, while the practical monitoring area and meteorological satellite data are quite different from the circumstance of original technique, it can not be directly applied to the operational drought monitoring. Therefore, the establishment of a national operational drought monitoring system will be the essential goal of this project. This system should directly serve the decision-makers by providing actual drought information. The imported technique will be coupled into the ongoing drought monitoring system to produce daily nationwide drought severity distribution and statistical results. This future system will be the combination of large-scale satellite remote sensing data, a hydrological model and meteorological data and can be used in practical operation to monitor the nationwide drought disaster.

2 Theory and methodology

2.1 Surface Energy Balance System (SEBS) and relative evaporation

The Surface Energy Balance System (SEBS) has been developed by Dr. Z. Bob Su and colleagues of the Satellite Earth Observation – Researches into Water, Climate and Environment (SEO-WaterCliEnt) research group of Wageningen University & Research Centre (Z. Su et al., 1998; Z. Su, 2001, 2002). Using visible and infrared satellite remote sensing data, SEBS is based on land surface energy balance theory combined with the in-situ meteorological data or the product of atmospheric numerical model to estimate land surface turbulent flux and the relative evaporation at different scales.

Infrared radiance is a function of the land surface brightness temperature, which in turn is an instantaneous observation to the land surface energy balance. The land surface balance is driven by the net radiation that is controlled by solar radiation at daytime. At any moment, the net radiation can be partitioned into sensible heat flux, latent heat flux and soil heat flux as the following equation

$$R_n = G_o + H + \lambda E \tag{2.1}$$

where R_n is net radiation, G_0 is soil heat flux, H is sensible heat flux which is the energy to heat up the surrounding air temperature, λ is the heat of vaporization that refers the heat used to change liquid water to vapor per volumetric unit, E is the amount of evaporation, λE is the corresponding latent heat flux.
Net radiation is expressed as the following equation

$$\begin{aligned} R_n &= K^{\downarrow} - K^{\uparrow} + L^{\downarrow} - L^{\uparrow} \\ &= (1-\alpha)R_{sw} + \varepsilon(\varepsilon'\sigma T_a^4 - \sigma T_0^4) \end{aligned} \tag{2.2}$$

where $K^{\downarrow}, K^{\uparrow}, L^{\downarrow}$ and $L^{\uparrow}$ are downward, upward shortwave radiation, downward and upward longwave radiation, α is land surface albedo, R_{sw} is downward solar radiation, σ is the Stefan-Bolzmann constant, ε is the emissivity of the land surface, ε' is the emissivity of the atmosphere, T_a is air temperature, and T_0 is the surface temperature.
The soil heat flux is parameterized as

$$G_o = R_n.[\Gamma_c + (1-f_c).(\Gamma_s - \Gamma_c)] \tag{2.3}$$

where $\Gamma_c = 0.05$ for full vegetation canopy (Monteith, 1973) and $\Gamma_s = 0.315$ for bare soil (Kustas and Daughtry 1989), f_c is the fractional canopy coverage.

$R_n - G_0$ is land surface effective energy which is the sum of sensible heat flux and latent heat flux. The key for the determination of land surface temperature is the partition of sensible and latent heat flux, which is controlled by the available water amount transferred from land into the atmospheric layer via the evaporation process. Therefore, λE and E can be estimated from the estimated land surface temperature.

The relative evaporation is the ratio between the actual evaporation and the potential evaporation. The actual evaporation is determined by the potential evaporation which is controlled by meteorological condition (air temperature, wind, solar radiation and humidity, etc.) and soil water content. Therefore, the relative evaporation reveals the actual moisture status of the soil. As a result, the drought severity can be assessed from the comparison between relative evaporation and other measurement data of soil moisture status, when the relative evaporation can be estimated from the combination of remote sensing data and meteorological data.

2.2 Methodology for estimating the relative evaporation from SEBS

The relative evaporation can be estimated from SEBS in following four steps: the retrieval of land surface parameters; the computation of friction wind velocity, sensible heat flux and stability length; the estimation of momentum and heat transfer roughness; the computation of relative evaporation.

2.2.1 Determination of land surface parameters

This system requires parameters including solar radiation, surface albedo, vegetation index, land surface emissivity and land surface temperature.
Solar radiation:

$$R_{sw} = I_{sc} \cdot e_0 \cdot \cos\theta_z \cdot \exp(-m \cdot \tau) \tag{2.4}$$

where I_{sc} is the solar constant, e_0 is the eccentricity factor, θ_z is the solar zenith angle, m is the air mass, τ is the optical thickness.
Albedo (Valiente et al., 1995):

$$\alpha = 0.545 \cdot r_1 + 0.320 \cdot r_2 + 0.035 \tag{2.5}$$

where r_1, r_2 are the AVHRR band 1 and 2 surface reflectance after corrections of atmospheric effect and bi-directional effect.
Normalized Difference Vegetation Index (NDVI):

$$NDVI = \frac{r_2 - r_1}{r_2 + r_1} \tag{2.6}$$

Land surface emissivity (Caselles and Sobrino, 1989):

$$\varepsilon = \varepsilon_v f_c + \varepsilon_g (1 - f_c) + 4 < d\varepsilon > f_c (1 - f_c) \tag{2.7}$$

where $f_c = \dfrac{NDVI - NDVI_{\min}}{NDVI_{\max} - NDVI_{\min}}$ is vegetation fractional coverage, $< d\varepsilon >$ is a non-linear parameter (0.002), ε_v and ε_g are emissivity for vegetation and ground respectively in 10.5-12.5 μm spectral range, $\varepsilon_v = 0.985 \pm 0.007$, $\varepsilon_g = 0.960 \pm 0.010$.
Land surface temperature (Coll and Caselles, 1997)

$$T_0 = T_4 + [1.34 + 0.39 \times (T_4 - T_5)] \times (T_4 - T_5) + 0.56 + \alpha \times (1 - \varepsilon) - \beta \times \Delta\varepsilon$$
$$\alpha = W^3 - 8W^2 + 17W + 40 \tag{2.8}$$
$$\beta = 150 \times (1 - W/4.5) \quad (\text{W: g/cm}^2)$$

where T_4 & T_5 are the brightness temperature in NOAA/AVHRR in band 4 & 5, W is the atmospheric water vapour content, Δε is the spectral emissivity difference of NOAA/AVHRR band 4 & 5,

2.2.2 Determination of friction velocity, sensible heat flux and stability length with bulk atmosphere similarity theory

The sensible heat flux can be derived from the bulk atmosphere similarity theory. In the Atmospheric Surface Layer (ASL), the similarity relationships for the profiles of the mean wind speed and the mean temperature are usually written in integral form as

$$u = \frac{u_*}{k}\left[\ln\left(\frac{z - d_0}{z_{0m}}\right) - \Psi_m\left(\frac{z - d_0}{L}\right) + \Psi_m\left(\frac{z_{0m}}{L}\right)\right] \tag{2.9}$$

$$\theta_0 - \theta_a = \frac{H}{k u_* \rho C_p}\left[\ln\left(\frac{z - d_0}{z_{0h}}\right) - \Psi_h\left(\frac{z - d_0}{L}\right) + \Psi_h\left(\frac{z_{0h}}{L}\right)\right] \tag{2.10}$$

where $u_* = (\tau_0/\rho)^{1/2}$ is the friction velocity, ρ is the density of air, k is van Karman constant, C_p is specific heat at constant pressure, height z is measured above the surface, d_0 is the zero plane displacement height, z_{0m} is the roughness height for momentum transfer, θ_0 is the potential temperature at the surface, θ_a is the potential temperature of the air, z_{0h} is the scalar roughness height for heat transfer, ψ_m and ψ_h are the stability correction functions for momentum and sensible heat transfer respectively, L is the Obukhov length defined as

$$L = -\frac{\rho C_p u_*^3 \theta_v}{kgH} \tag{2.11}$$

where g is the acceleration due to gravity, and θ_v is the potential virtual temperature near the land surface.

The wind friction velocity u_*, stability length L and sensible heat flux H can be obtained by solving the system of non-linear Equations (2.9-2.11) using the method of Broyden iteration.

2.2.3 Determination of roughness length for momentum and heat transfer

The roughness lengths for momentum and heat transfer must be determined in advance in above equations. They are generally parameterized with the ground measured meteorological data. However, they are difficult to obtain for large-scale application where the ground-measured data are not sufficient.

Parameterisation models for estimation of the roughness lengths for momentum and heat transfer have been developed based on the remote sensing data to solve these two parameters.

The momentum transfer roughness lengthen can be derived from its relationship with vegetation index (Su, 2001)

$$Z_{0m} = 0.0005 + 0.5 \times \left(\frac{NDVI}{NDVI_{\max}} \right)^{2.5} \tag{2.12}$$

Then, the zero-plane displacement height $d_0 = Z_{0m} \times 4.9$, vegetation height $h = Z_{0m}/0.136$. Heat transfer roughness length can be derived from the following equation $Z_{0h} = Z_{0m}/\exp(kB^{-1})$, where B^{-1} is a dimensionless heat transfer coefficient.

The model proposed by Su et al. (2001) is used to estimate kB^{-1}

$$kB^{-1} = \frac{kC_d}{4C_t \frac{u_*}{u(h)}\left(1 - e^{-n/2}\right)} f_c^2 + \frac{k \cdot u_* / u(h) \cdot z_{0m} / h}{C_t^*} f_c^2 f_s^2 + kB_s^{-1} f_s^2 \tag{2.13}$$

where f_c is the fractional canopy coverage and f_s is its compliment. C_d is the drag coefficient of the foliage elements assumed to take the value of 0.2. C_t is the heat transfer coefficient of the leaf assumed to take a value of 0.01. $u(h)$ is the horizontal

wind speed at the canopy top. The heat transfer coefficient of the soil is given by $C_t^* = \mathrm{Pr}^{-2/3}\,\mathrm{Re}_*^{-1/2}$, where $\mathrm{Pr}=0.71$ is the Prandtl number and the roughness Reynolds number $\mathrm{Re}_* = h_s u_* / \nu$, with h_s the roughness height of the soil. The kinematic viscosity of the air is given by $\nu = 1.327 \cdot 10^{-5}(p_0/p)(T/T_0)^{1.81}$ (Massman, 1999), p and T are the ambient pressure and temperature, $p_0 = 101.3$ kPa and $T_0 = 273.15$ K. For bare soil surface kB_s^{-1} is calculated according to Brutsaert (1982):

$$kB_s^{-1} = 2.46(\mathrm{Re}_*)^{1/4} - \ln[7.4] \tag{2.14}$$

In equation (2.13), the within-canopy wind speed profile extinction coefficient n is formulated as a function of the cumulative leaf drag area at the canopy top expressed as (Su et al., 2001):

$$n = \frac{C_d \cdot LAI}{2u_*^2 / u(h)^2} \tag{2.15}$$

where $LAI = \left[NDVI \times \frac{1 + NDVI}{1.000001 - NDVI} \right]^{0.5}$ is vegetation leaf area index.

2.2.4 Relative evaporation estimated from the limiting conditions in the land surface energy balance

The latent heat flux can be theoretically derived from equation (2.1) with the computed sensible heat flux. However, this computation is based on the ground measured wind speed and air temperature, the uncertainties in the observed data will cause error in the sensible heat flux and affect the latent heat flux furthermore. In SEBS, the error will be constrained within an range based on the computation of the sensible heat flux in the extreme dry and wet conditions, based on the characteristic of sensible heat flux in the extreme dry and wet condition, which will obviously enhance the reliability for the computed results.
In the extreme dry condition, the latent heat flux or evaporation will be zero because of soil water content becomes zero, the following equation can be derived from (2.1)

$$\lambda E_{dry} = R_n - G_0 - H_{dry} \equiv 0, \text{ or}$$
$$H_{dry} = R_n - G_0 \tag{2.16}$$

In the extreme wet condition, the actual evaporation will be equal to the potential evaporation entirely determined by atmospheric conditions. The sensible heat flux will achieve its minimum

$$\lambda E_{wet} = R_n - G_0 - H_{wet}, \text{ or}$$
$$H_{wet} = R_n - G_0 - \lambda E_{wet} \tag{2.17}$$

The relative evaporation will be

$$\Lambda_r = \frac{\lambda E}{\lambda E_{wet}} = 1 - \frac{\lambda E_{wet} - \lambda E}{\lambda E_{wet}} \tag{2.18}$$

Combine (2.1), (2.16), (2.17) and (2.18), the relative evaporation can be expressed as

$$\Lambda_r = 1 - \frac{H - H_{wet}}{H_{dry} - H_{wet}} \tag{2.19}$$

Simultaneously, we can define the Drought Severity Index (DSI) as

$$DSI = 1 - \Lambda_r = \frac{H - H_{wet}}{H_{dry} - H_{wet}} \tag{2.20}$$

The sensible heat flux H has been constrained within H_{dry} and H_{wet}, H_{dry} can be derived from (2.16), H_{wet} will be derived from the combination of (2.17) and Penman-Monteith equation (Monteith, 1965) as the following form

$$\lambda E = \frac{\Delta \cdot r_e \cdot (R_n - G_0) + \rho C_p \cdot (e_{sat} - e)}{r_e \cdot (\gamma + \Delta) + \gamma \cdot r_i} \tag{2.21}$$

where e and e_{sat} are vapor pressure and saturated vapor pressure respectively; γ is the psychometric constant, Δ is the rate of change of saturation vapor pressure with temperature, r_i is the bulk surface internal resistance and r_e is the external or aerodynamic resistance. The difficulty to evaluate latent heat flux lies in the fact that the internal resistance, r_i, is generally regulated by the internal surface moisture availability which is in turn influenced by evaporation. Therefore, the direct computation of latent heat flux using r_i is not recommendable.

For completely wet land surface, per definition it is assumed that r_i = 0, the sensible heat flux can be written as following according to (2.21)

$$H_{wet} = \left((R_n - G_0) - \frac{\rho C_p}{r_{ew}} \cdot \frac{e_s - e}{\gamma} \right) \Big/ \left(1 + \frac{\Delta}{\gamma} \right) \tag{2.22}$$

where the external resistance in the extreme wet condition are

$$r_{ew} = \frac{1}{ku_*}\left[\ln\left(\frac{z-d_0}{z_{0h}}\right) - \psi_h\left(\frac{z-d_0}{L_w}\right) + \psi_h\left(\frac{z_{0h}}{L_w}\right)\right] \tag{2.23}$$

The stability length in the extreme wet condition is

$$L_w = -\frac{\rho u_*^3}{kg \cdot 0.61 \cdot (R_n - G_0)/\lambda} \tag{2.24}$$

Once H_{wet} has been determined, the relative evaporation Λ_r and latent heat flux λE can be derived.

3 Data processing and actual computation

3.1 Data descriptions

As the requirements of this project, large-scale real-time datasets need to be collected when applying SEBS to large-scale drought monitoring, with which various parameters relevant to the relative evaporation can be estimated, while some other parameters need to be set by parameterization schemes.

NOAA/AVHRR is the US Polar Orbiting Meteorological Satellite series, two NOAA satellites can observe one location four times every day, with overpasses at 2:00, 8:00, 14:00 and 20:00 local time respectively. The spatial resolution of AVHRR data is 1.1 kilometer in five channels, two channels in visible bands, one channel in near infrared band, and the other two channels in thermal infrared bands. Land surface albedo, temperature, vegetation index and land surface emissivity can be estimated from the satellite observation data. The air temperature, water vapor and wind speed can be extracted from ground measured meteorological database. Table 3.1 is the required variables and their sources. The following data need to be prepared.

1. Remote sensing data: NOAA/AVHRR data in Channels 1, 2, 4 and 5.
2. Ground measured data: seal level air pressure, air temperature, dew-point air temperature, wind speed and visibility.
3. Other data: Coordinates and altitude of the meteorological stations and observational time and date.

Table 3.1 SEBS input variables and their sources

Symbol (unit)	Variable or parameter	Source or parameterisation
$\alpha(-)$	Albedo	AVHRR data in channels 1, 2
$NDVI(-)$	Normalized difference vegetation Index	AVHRR data in channels 1, 2
$\varepsilon(-)$	Emissivity	NDVI
$\varepsilon'(-)$	Atmospheric emissivity	$9.26\times10^{-6}\times T_a^2$
$f_c(-)$	Vegetation fractional coverage	NDVI
$LAI(-)$	Leaf area index	NDVI
$z(m)$	PBL depth	1000
$d_0(m)$	Displacement height	$z_{0m}\times4.9$
$z_{0m}(m)$	Roughness length for momentum transfer	NDVI
$z_{0h}(m)$	Roughness length for heat transfer	Model computation
$u(ms^{-1})$	PBL wind speed	Ground measured wind speed
$u(h)(ms^{-1})$	Wind speed at the top of canopy	u, d_0, z_{0m}
$T_0(^0K)$	Land surface temperature	AVHRR data in channels 4, 5
$T_a(^0K)$	Air temperature at PBL height	Ground measured air temperature
$p_a(pa)$	Air pressure at PBL height	Sea level air pressure and altitude of the observation site
$e_s(pa)$	Saturation vapor pressure	T_0, T_a
$e(pa)$	Actual vapor pressure	Land surface air temperature, dew-point air temperature, p_a
$\tau(-)$	Atmospheric optical thickness	Horizon visibility
$\theta_a(^0K)$	Potential air temperature	T_a, p_a, sea level air pressure
$\theta_0(^0K)$	Surface potential temperature	T_0, p_a, sea level air pressure
$\theta_v(^0K)$	Surface virtual potential temperature	θ_0, land surface dew-point temperature
$R_{sw}(Wm^{-2})$	Solar radiation	Year, Month, Date and time and $\tau(-)$

3.2 Data retrieval and pre-processing

The goal of this project is to establish a nationwide operational drought monitoring system. So, the data retrievals need to consider the following requirements: 1) the data should cover a sufficient long time period (two months); 2) The data should have large-scale regional coverage; 3) The satellite remote sensing data and ground measurement data should be approximately synchronous.

Based on the above requirements, the daily NOAA/AVHRR data in July and August 2000 have be collected, the satellite remote sensing data cover the central area of China with a east-west width of about 2000 kilometer. The daily ground meteorological data in the corresponding 600 sites have also been collected.

The data pre-processing includes two components: satellite remote sensing data and ground meteorological data.

3.2.1 satellite data processing

1. The AVHRR 1B data are processed with ENVI package in following two steps
(1) Radiation calibration: The NOAA/AVHRR 1B data are converted into planetary reflectance in channel 1&2 and Kelvin brightness temperature in channel 3, 4, 5 with ENVI "Calibrate Data" module.
(2) Geometry calibration: The pixel geographic location, solar and satellite zenith angles can be derived from AVHRR 1B data with ENVI "Build Geometry File" module.
2. The correction of bi-directional effect in AVHRR channel 1&2:
The band-integrated radiance received at the satellite I^s can be modeled as the sum of five terms as following

$$I^s = I^{dir} + I^{sca} + I^{sky} + I^{ind} + I^{mul} \tag{3.1}$$

where I^{dir} is the radiation directly reflected by the ground from the solar beam towards the satellite; I^{sca} is the radiation singly scattered directly to the satellite sensor by the molecules and particles within the atmosphere; I^{sky} is the radiation singly scattered into a diffuse flux which impinges on the ground and then is reflected directly to the satellite; I^{ind} is the radiation reflected by the ground and subsequently scattered towards the satellite; I^{mul} is the contribution from all higher orders of molecular multiple scattering. The surface bi-directional reflectance is given by Paltridge and Mitchell (1990)

$$r = \frac{K(1-M) - \sec\phi_s \sum_{j=0}^{1} \Phi_j Q_j(m)}{4\cos\theta \cdot g(m) e^{-m\tau}(1+m\tau)} \tag{3.2}$$

where K is the AVHRR-measured value, θ, ϕ_s are the relevant angles associated with the measurement, M is the contribution from molecular multiple scattering, $Q_j(m)$ are the integrated source functions, g is related to air mass m which is the total air mass from the sun to ground to satellite, and τ is the aerosol optical depth. Φ is the phase function for air molecular and aerosol scattering.

3.2.2 Pre-processing the meteorological data

The meteorological data need to be interpolated and converted to match the satellite data before they are imported into SEBS.

1. Data interpolation
   The large amount of ground measured meteorological data are required to compute the regional relative evaporation in SEBS. The ground-measured data will be interpolated into image format which are consistent with the corresponding satellite pixels in geographic coordinate. In this project, the ground measured meteorological data are interpolated with a Distance Weighing algorithm.
2. Data conversion
   As shown in table 2.1, the most meteorological parameters needed in the calculation are not direct measurables, instead they are calculated or converted from the measured parameters. Therefore, the data conversion is a key pre-process. The detailed schemes are shown as below

Surface air pressure:

$$P_s = P_0\left(1-\frac{alt}{44331}\right)^{(1/0.1903)} \quad (Pa) \tag{3.3}$$

where P_0 is the sea level air pressure, alt is the altitude of observation sites.

Saturation vapor pressure:

$$e_s = 611\exp\left(\frac{17.502\times T_a}{240.97+T_a}\right) \quad (Pa) \tag{3.4}$$

where T_a is air temperature measured in near surface layer.

Actual vapor pressure:

$$e = 611\exp\left(\frac{17.502\times Tdewpt}{240.97+Tdewpt}\right) \quad (Pa) \tag{3.5}$$

where $Tdewpt$ is the measured dew-point temperature in near surface layer.

Specific humidity:

$$q = (R_d/R_v)\times e/P_s \quad (Kg/Kg) \tag{3.6}$$

where R_d, R_v are the gas constants for the dry air and water vapour air.

Potential temperature in near surface layer:

$$\theta_a = T_a\left(\frac{P_s}{P_0}\right)^{-0.286} \quad (K) \tag{3.7}$$

Virtual potential temperature in near surface layer:

$$\theta_v = T_a \times (1+0.61\times q)\times\left(\frac{P_s}{P_0}\right)^{-0.286} \quad (K) \tag{3.8}$$

3.3 Computational process and results

3.3.1 Initiation of the SEBS parameters

Many variables involved in SEBS applications need to be initiated, some of these parameters are physical parameters, others are empirical constants. Table 3.2 lists all these variables and their default values.

Table 3.2 SEBS parameters

Symbol (unit)	Parameters	Values or default value
$I_{sc}(Wm^{-2})$	Solar constant	1367.0
$W(g/cm^2)$	Air water vapor	1.92
$\Delta\varepsilon(-)$	Spectral emissivity difference of AVHRR band 4 & 5	0.002
$\varepsilon_v(-)$	Vegetation emissivity	0.98
$\varepsilon_s(-)$	Soil emissivity	0.95
$z(m)$	PBL depth	1000.
$\gamma(PaK^{-1})$	Psychrometric constant	67.
$R_v(Jkg^{-1}K^{-1})$	Water vapour gas constant	461.5
$R_d(Jkg^{-1}K^{-1})$	Dry air gas constant	287.04
$C_p(Jkg^{-1}K^{-1})$	Specific heat at constant pressure	1005.
$\lambda(Jkg^{-1})$	Latent heat of water vaporization	2.43×10^6
$g(ms^{-2})$	Gravitational acceleration	9.8
$\sigma(Wm^{-2}K^{-4})$	Stefan-Bolzmann constant	5.678×10^{-8}
$k(-)$	Von Karman constant	0.41

3.3.2 Computational process

SEBS code is written in IDL language and need to be applied under ENVI software platform. The computation consists of three parts, which are the data pre-processing, land surface parameter retrieval and the computation of relative evaporation. The whole process are divided into eight steps as given in the following flowchart:

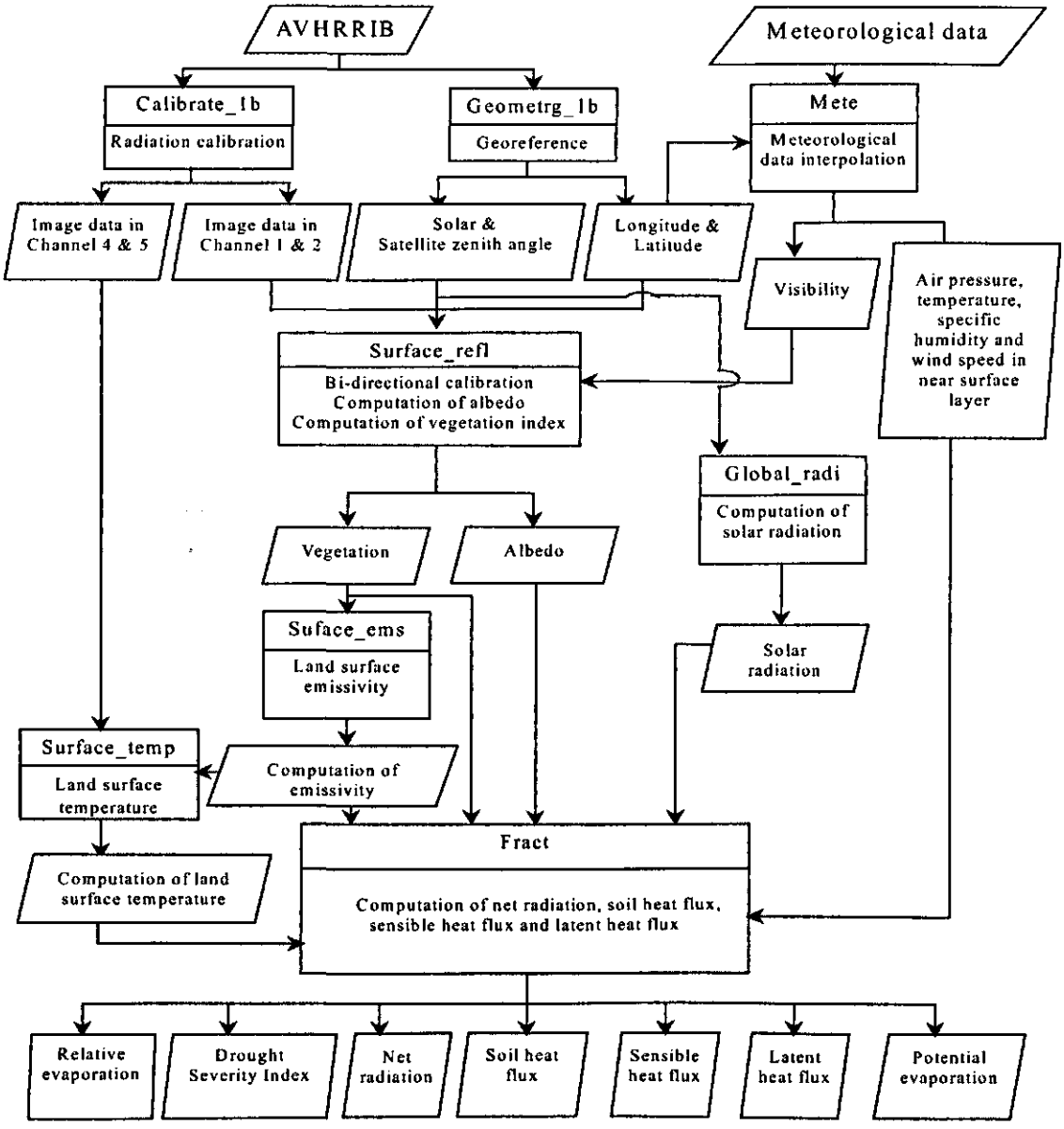

Figure 3.1. SEBS flowchart

3.3.3 Computational results

The outputted SEBS results are listed as the following 12 files, all are given in image format which can be viewed in ENVI (Table 3.3).

Table 3.3 the outputted results of SEBS

SN	File name	Variables
1	Relative_evaporation	Relative evaporation
2	Drought_severity_index(DSI)	Drought severity index
3	Net_radiation	Net radiation
4	Soil_heat_flux	Soil heat flux
5	Sensible_heat_flux	Sensible heat flux
6	Latent_heat_flux	Latent heat flux
7	Potential_evaporation	Potential evaporation
8	Global_radiation	Global radiation
9	Broad_band_albedo	Broadband albedo
10	Emissivity	Emissivity
11	NDVI	Vegetation index
12	Land_surf_temp	Land surface temperature

4 Validation and analysis of the results

4.1 Validation scheme

As SEBS can output plenty of parameters and its regional computation will take long time, it is difficult to obtain all the required large amount of ground measured data for validation. Therefore, this project will only focus on the relative evaporation analysis, which can directly reflect the drought severity.

In order to examine the feasibility to apply SEBS in the operational application in combination with the ongoing drought monitoring system, this project will focus on the comparison between SEBS results and the soil water deficit derived from the ongoing drought monitoring system to validate the final results.

4.1.1 Introduction of the soil water deficit monitoring algorithm

This algorithm has been developed in WRIC/MWR in order to monitor the nationwide large-scale drought disaster. It is based on the combination of a hydrological model and meteorological data to derive the nationwide soil water deficit, to classify and assess the drought severity according to the relationship between the soil water deficit and local drought severity. Since the establishment of the ongoing system in 1996, several hydrological and meteorological outputs are continuously produced based on daily iteration of routine meteorological data. The outputs of the system have been used in operational flood and drought prevention for more than six years, the results of which show that it is feasible to monitor the drought with the combination of a hydrological model and meteorological data. However, because there is no regional remote sensing data as a reference and the hydrological model did not take the spatial variation of land surface into account, the spatial resolution of the products of this ongoing system is very low and serious discrepancy exist between products of the system and the actual drought severity.

This ongoing system consists of two parts: (1) The computation of potential evaporation; (2) The computation of soil water deficit. The potential evaporation is computed from Penman equation. According to application requirements, the daily potential evaporation is computed from in-situ air temperature, wind speed, humidity and cloud coverage over the nationwide 600 ground sites, then the results are presented to the users in interpolated map format (Zhou et al., 1998). The daily local soil water deficit is derived from a model on the basis of runoff generated by infiltration-excess and moisture depletion with the estimated local potential evaporation and the measured local precipitation (Yan et al., 1997). The underlying soil is considered as "ideal" which there is no irrigation, no vegetation and representative of the area surrounding the concerned meteorological station. Drought severity is derived by assessing history data.

4.1.2 Validation scheme

The daily soil water deficit from the ongoing operational system and SEBS produced relative evaporation for the 600 ground sites will be extracted for the period from July to August 2000. Correlation analysis will be performed to these data in the following sections.

4.2 Validation result

4.2.1 Comprehensive analysis

The test area covers 27-41°N and 105-126°E region. As the limited coverage of the satellite data, cloud condition and other reasons related to missing data, only 24 satellite scenes are available for this comparison, 68.5 sites are located within the test area on average, which is about 48.5 % of the entire calculation domain. The values of outputted SEBS results used are ranged from 0 to 1.05.

4.2.2 Correlation analysis

The soil water deficit data are extracted corresponding to the geographic locations of the SEBS computed relative evaporation. The relationship between the plant available water and Drought Severity Index (converted from SEBS derived relative evaporation) are presented in Figure 4.1, where R^2 is a statistical parameter valued between 0 and 1, which reveals how closely the estimated values for the trend-line correspond to the actual data. The trend-line is most reliable when R-squared value is at or near 1. This correlation passes the linear correlation test. The negative correlation coefficient means that the relationship between the soil water deficit and computed relative evaporation is correct. The correlation is worse in the eastern plain area than the middle area.

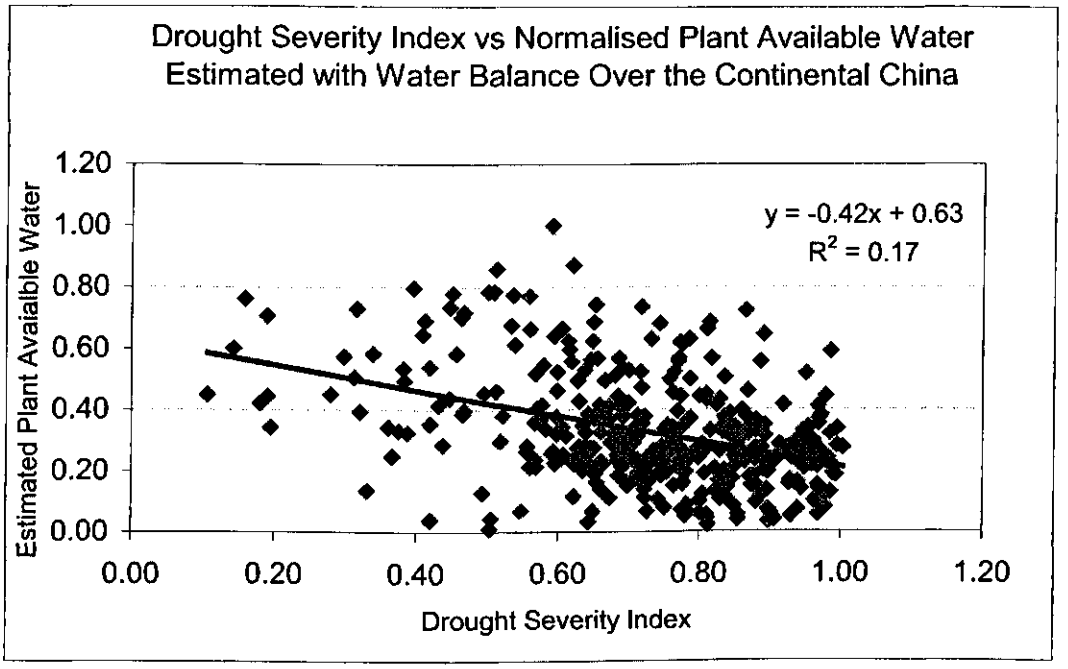

Figure 4.1. Drought Severity Index vs Normalised Plant Available Water Estimated with Water Balance Over the Continental China

4.2.3 Cases study

4.2.3.1 Daily analysis at the individual site

The results are not ideal when two outputs are compared in temporal scale, even weak positive correlation occurs at some sites, which means that the daily comparison between the two parameters is less successful for all sites simultaneously. If the data are extracted randomly for each site, the comparison results are better. The following figures give the relationships between the normalized plant available water index and drought severity index at several ground observation sites that also show the negative correlation (Figure 4.2). This indicates that DSI can effectively reflect the actual drought severity.

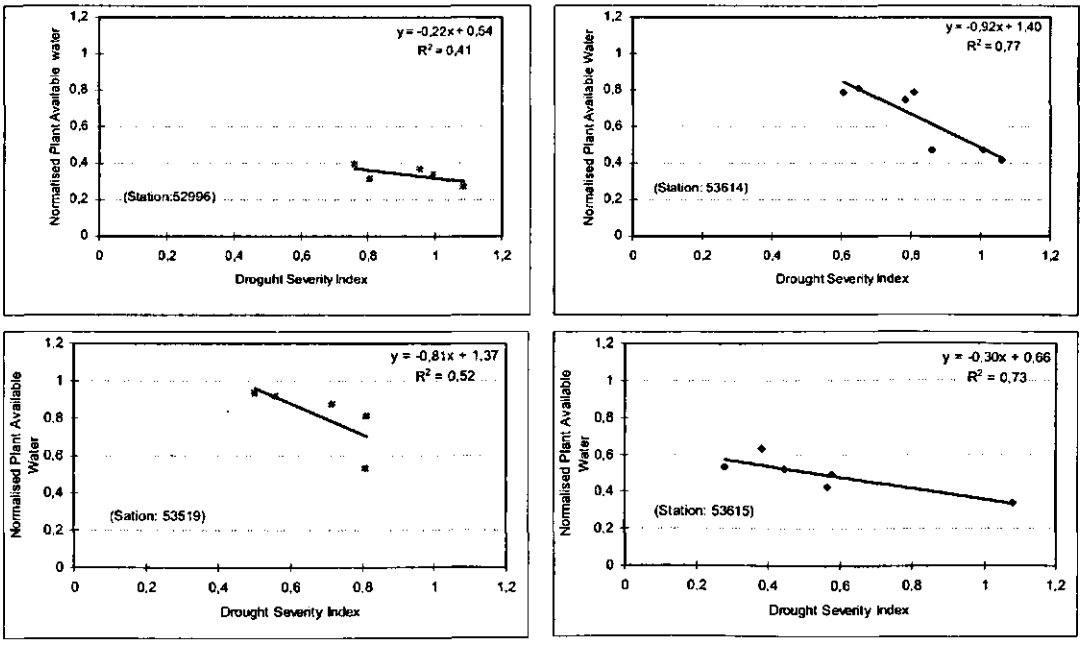

Figure 4.2. Drought severity index vs normalised plant available water estimated with water balance in several ground observation sites over the continental China

4.2.3.2 Regional analysis for individual day

In order to ana'yze the two outputs at regional scale, the cloud-free SEBS results and the corresponding soil water deficit data are extracted. As an example, the correlation coefficient reaches 0.59265 with 117 samples on July 8, 2000. To compare the drought response to the results of different methods, Figure 4.3 give the nationwide distributions of relative evaporation from SEBS, and hydrological and meteorological drought and soil water deficit derived from the WRIC/MWR system. It reveals that the three parameters derived from different methods are comparable, and the regional distributions are consistent in general. As the relative evaporation computation is based on the satellite remote sensing data, if the land surface is covered by cloud, it can not give the right situation on the land surface, however under cloud-free condition, the computed results are physically meaningful and the revealed spatial distributions must be judged physically realistic.

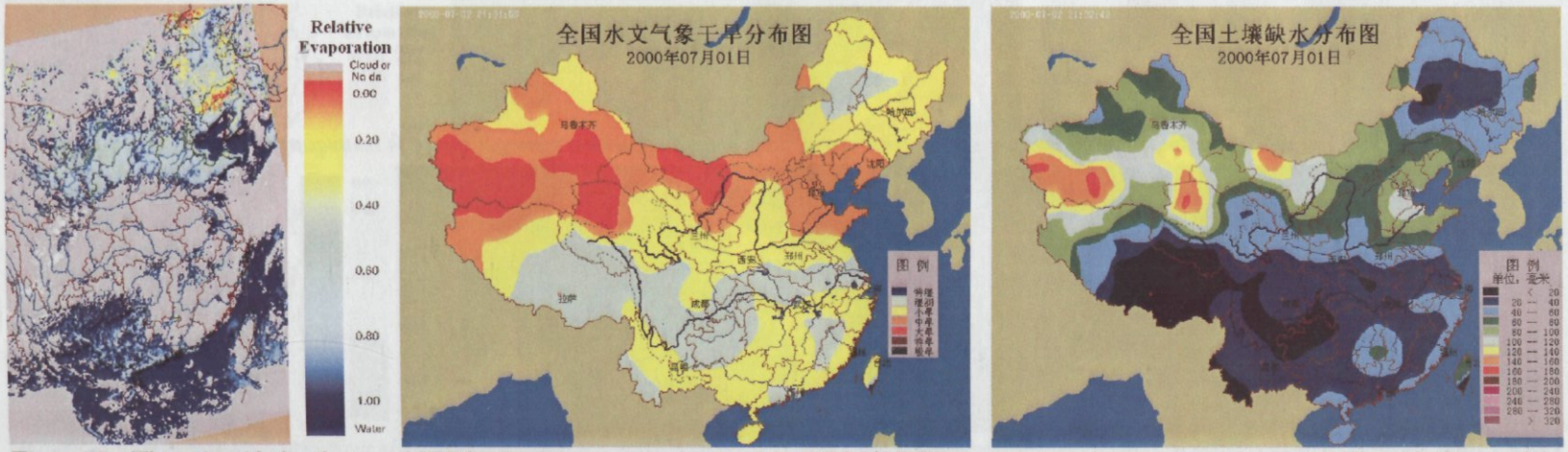

Figure 4.3a. The nationwide distributions of SEBS estimated evaporative fraction (left), WRIC/MWR system estimated meteorological drought (middle) and soil water deficit (right) on July 1, 2000

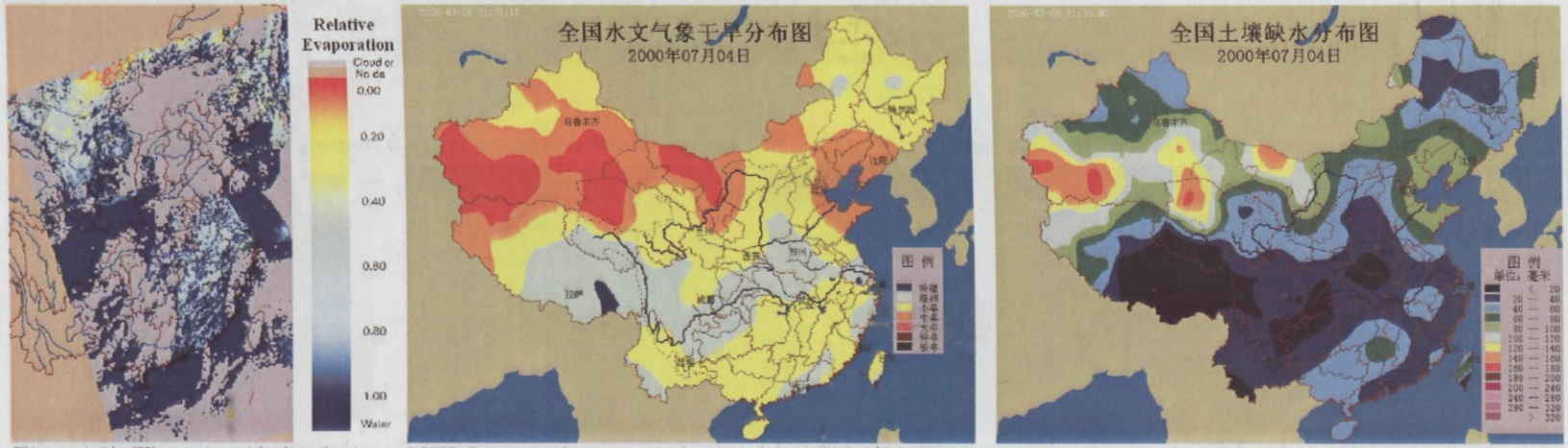

Figure 4.3b. The nationwide distributions of SEBS estimated evaporative fraction (left), WRIC/MWR system estimated meteorological drought (middle) and soil water deficit (right) on July 4, 2000

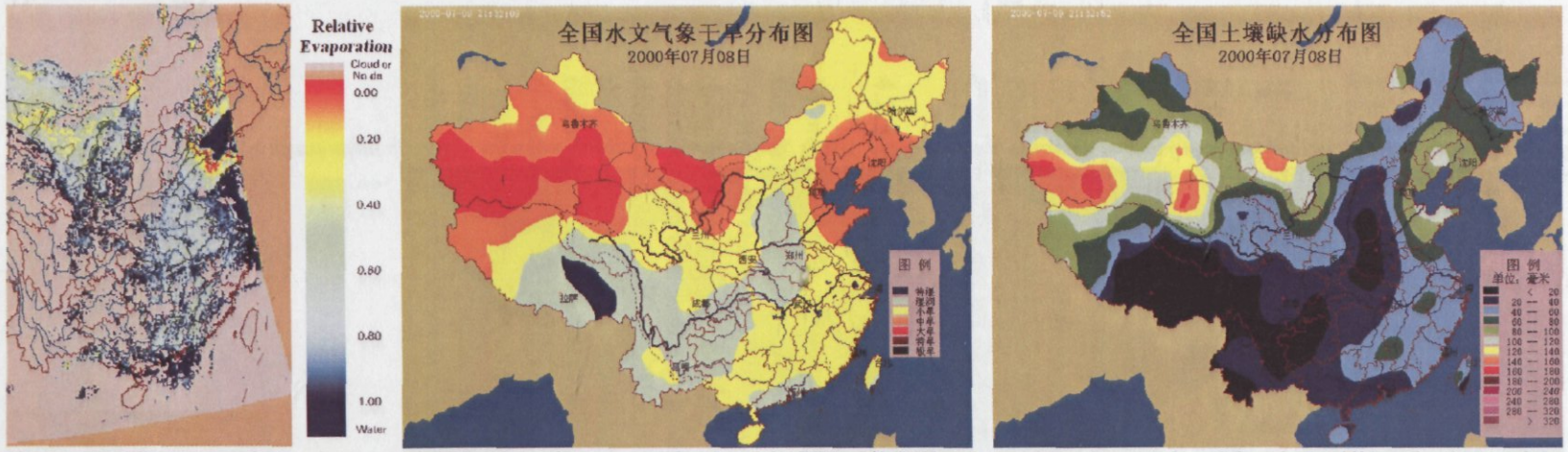

Figure 4.3c. The nationwide distributions of SEBS estimated evaporative fraction (left), WRIC/MWR system estimated meteorological drought (middle) and soil water deficit (right) on July 8, 2000

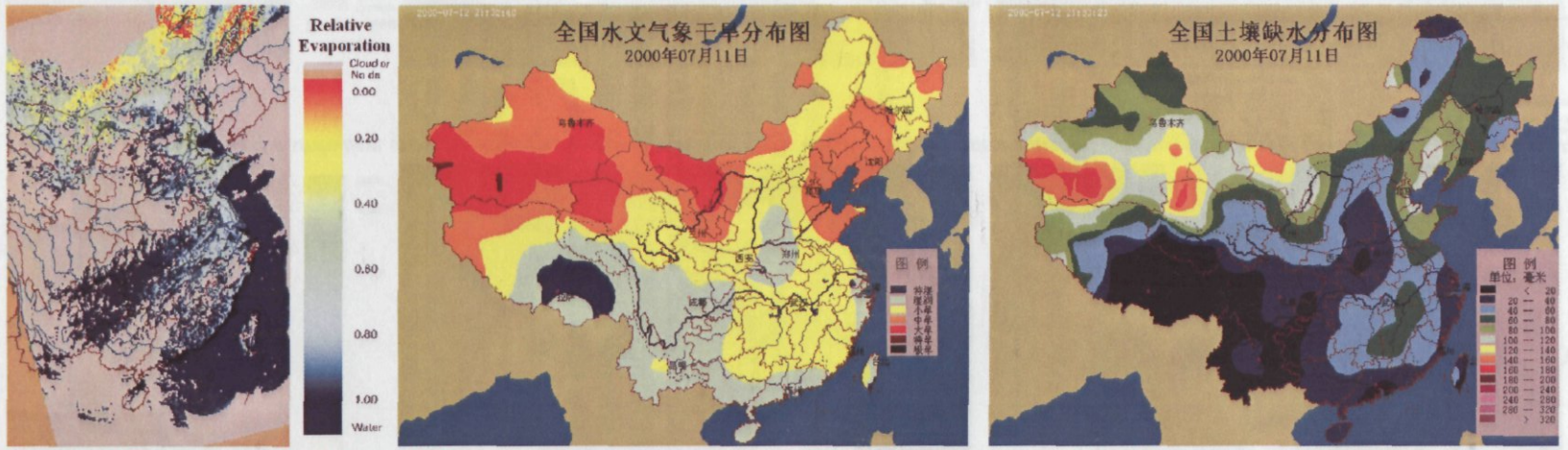

Figure 4.3d. The nationwide distributions of SEBS estimated evaporative fraction (left), WRIC/MWR system estimated meteorological drought (middle) and soil water deficit (right) on July 11, 2000

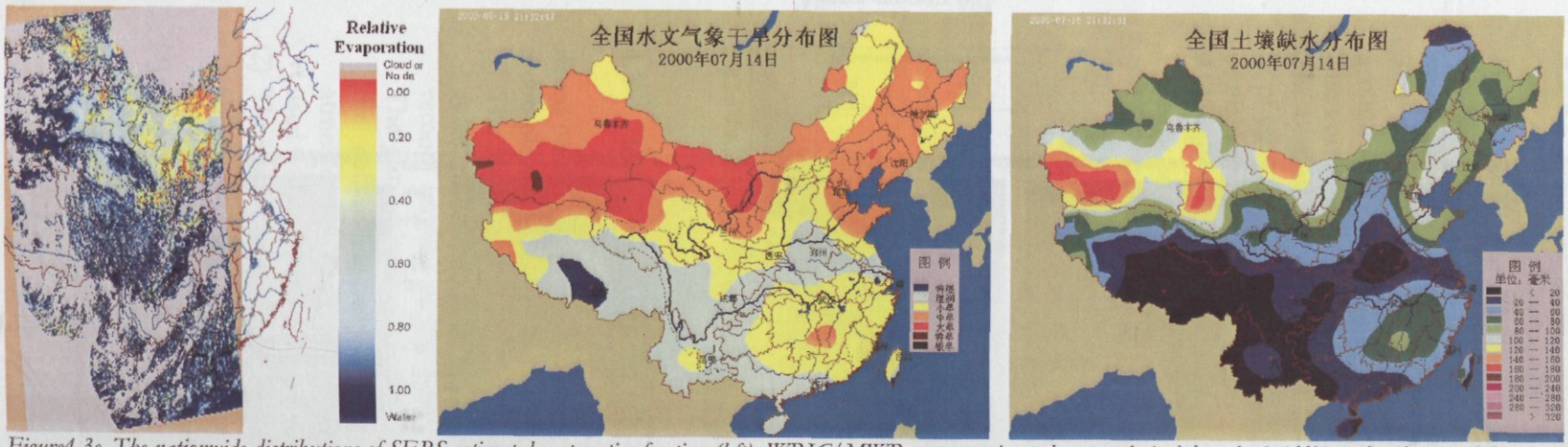

Figure4.3e. The nationwide distributions of SEBS estimated evaporative fraction (left), WRIC/MWR system estimated meteorological drought (middle) and soil water deficit (right) on July 14, 2000

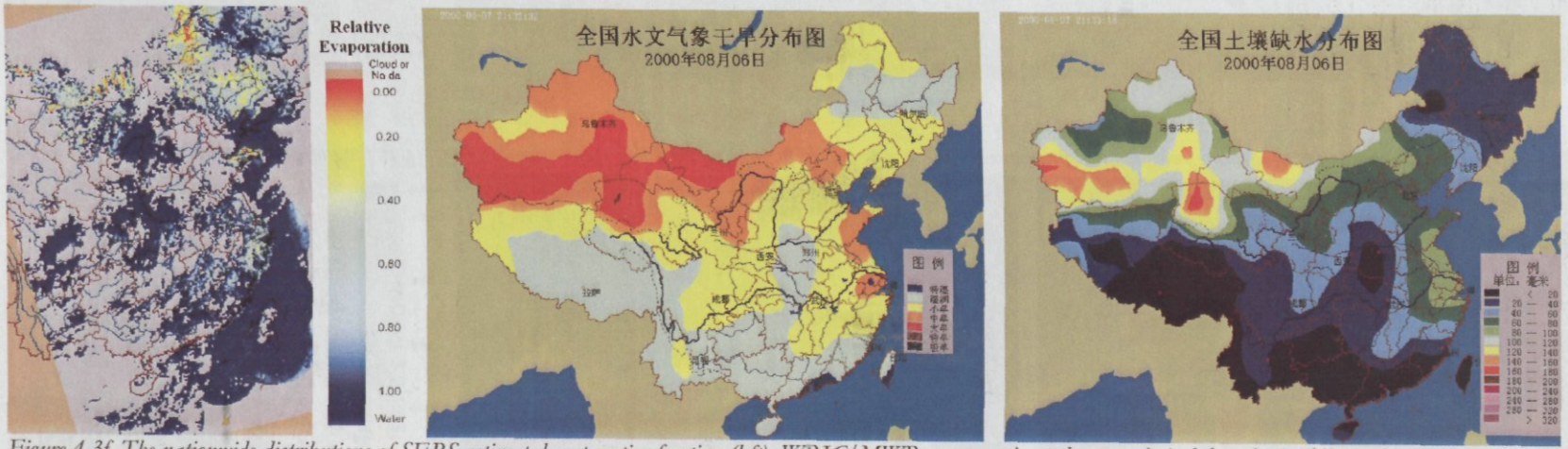

Figure 4.3f. The nationwide distributions of SEBS estimated evaporative fraction (left), WRIC/MWR system estimated meteorological drought (middle) and soil water deficit (right) on August 6, 2000

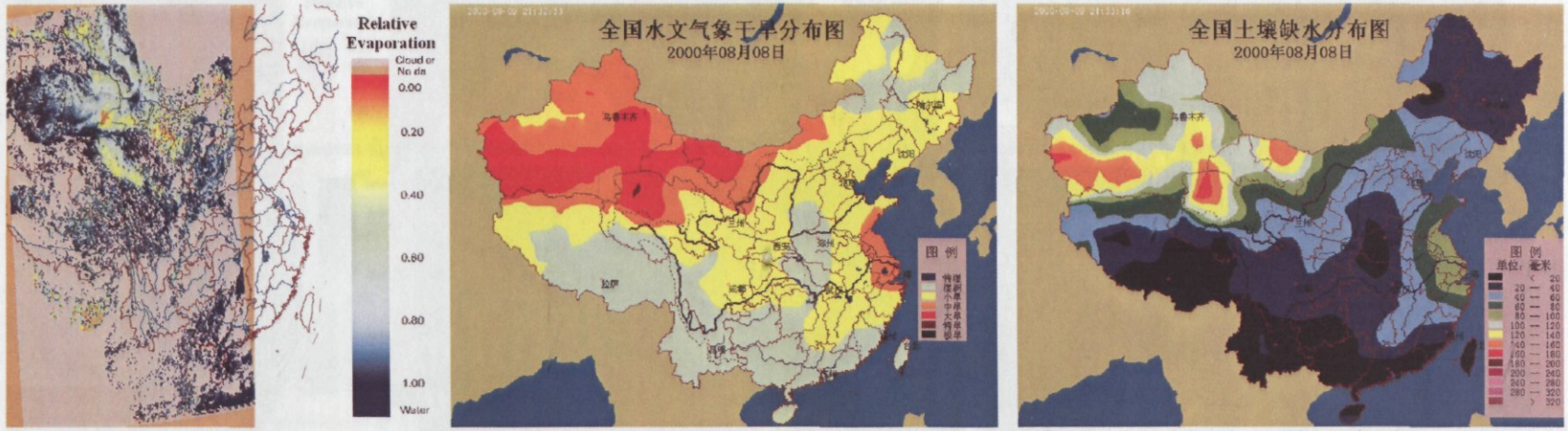

Figure 4.3g. The nationwide distributions of SEBS estimated evaporative fraction (left), WRIC/MWR system estimated meteorological drought (middle) and soil water deficit (right) on August 8, 2000

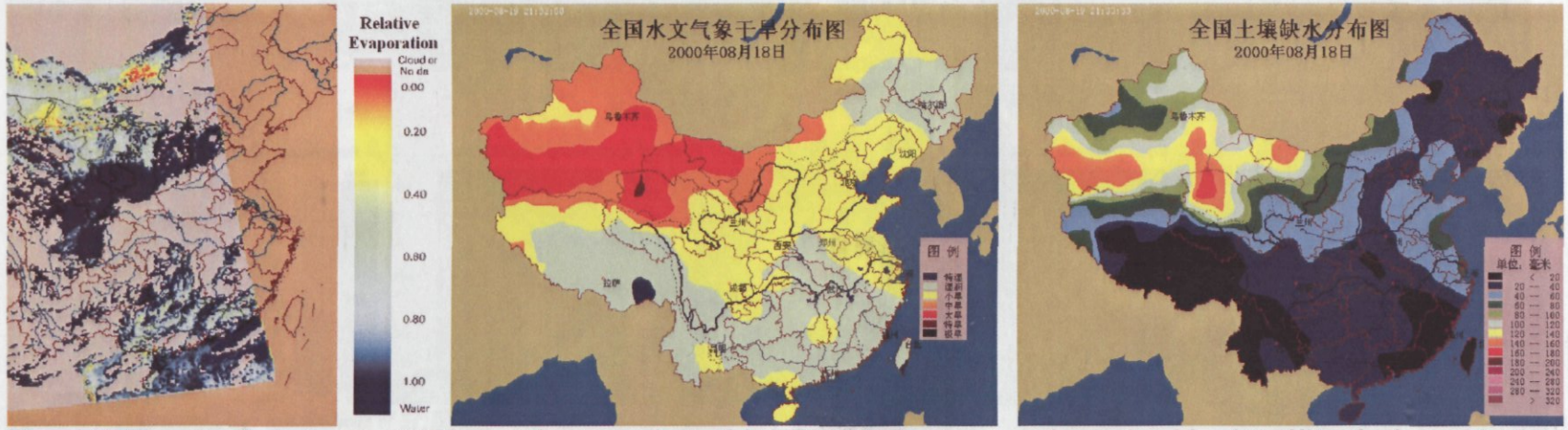

Figure 4.3h. The nationwide distributions of SEBS estimated evaporative fraction (left), WRIC/MWR system estimated meteorological drought (middle) and soil water deficit (right) on August 18, 2000

4.2.4 Typical comparison analysis

Here we take July 8, 2000 as an example again and choose one dry and one wet region from the output of the WRIC/MWR system as the dry and wet cases. The comparison will be performed as following.
The dry region covers the area within 35-41°N and 116-122°E with 20 available ground sites, the wet region covers 30-37°N and 110-116°E with 21 available sites. The correlation coefficients between the two outputs are 0.41 and 0.78 respectively. The corresponding average soil water deficits are 98.35 and 28.77 respectively which is physically very good and meaningful. The following Figure 4.4 gives the plant available water and drought severity index over North china and East China. Although R-square value is not high, the trend between plant available water and Drought Severity Index is consistent.

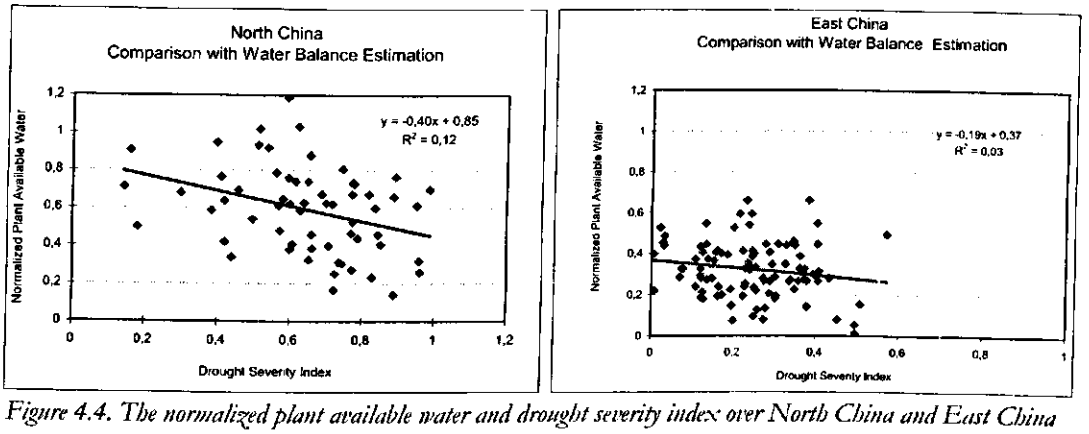

Figure 4.4. The normalized plant available water and drought severity index over North China and East China

4.3 Error analysis

Based on the above temporal and spatial analyses, it is concluded that the final result is completely satisfactory. The error maybe caused from following aspects:

(1) The implemented calibration or correction of satellite remote sensing data is not sufficient in this system. The bi-directional effect has been corrected in satellite remote sensing visible band, but the atmospheric correlation is not sufficient. The atmospheric aerosol and water vapor only take the empirical values, while the daily variations of these parameters are not considered. Because the atmospheric conditions are different from day to day, the fixed empirical values used will cause errors in the retrieved land surface parameters.

(2) The soil water deficit has its own error which is caused by the hydrological model and meteorological data, the uncertainty will occur when it is compared to SEBS computed relative evaporation.

(3) The computational process involves many steps. The error will be transferred and accumulated when the meteorological data are combined with the satellite remote sensing data, such that the final error of the system become not negligible.

(4) Some of the data are questionable to represent the practical situation of the corresponding parameters, which maybe an important error source.

4.4 Discussion and remark

(1) The relative evaporation gives zero values at some sites, which should be the extreme drought condition, but is practically not completely true. Because the computation of sensible heat flux is independent of the energy balance equation, the computed sensible heat flux may be greater than the available energy flux, consequently the computed relative evaporation will be considered zero in this case. This reminds that the computational algorithm of the sensible heat flux needs to be improved furthermore.

(2) The comparison results show that the computed relative evaporation is not sufficient yet for operational drought monitoring. First, because of cloud effects and the required ground measured meteorological data (for the derivation of atmospheric transmissivity), the area with usable results is less than half of the whole test area. Second, the comparison is not sufficiently consistent in temporal scale, which indicates that systematic error may exist between the daily observation data in temporal scale. The first reason maybe the key one. In addition, the correlation between the two outputs is not entirely satisfactory. Enhanced data pre-processing, combination with soil water deficit and application of the Harmonic ANalysis of Time Series (HANTS) tool for data analysis and interpolation of missing data will be the main task in the future.

5 Conclusion

In order to monitor the nationwide real-time large-scale drought disaster, this project has imported the advanced SEBS technique, which includes a set of tools for retrievals of land surface geo-physical parameters and uses the combination of the satellite remote sensing and ground measurement data to estimate regional relative evaporation. Because meteorological satellite data can cover large region with high overpass and economic cost, and the SEBS technique has clear physical mechanism and easy operational ability at the same time, the practical applicability of the technique is relatively high. During the importing process, the original techniques have been modified from the original small scale experiment to large-scale operational applications. The final results show that the implementation and modification are successful and the system can be used feasibly for operational large-scale drought monitoring. Nevertheless it is felt that the obtained results do not yet satisfy all the application requirements. Further modification and improvement are still necessary for real-time applications in the future. It is concluded that an operational nationwide real-time large-scale drought monitoring system can be established by combination and assimilation of the on-going drought monitoring system and the imported techniques.

References

Brutsaert, W., 1982: Evaporation into the atmosphere, Reidel, Dordrecht, 299 pp.

Brutsaert, W., 1998: Land-surface water vapor and sensible heat flux: Spatial variability, homogeneity, and measurement scales. Water Resour. Res., 34: 2433-2442.

Brutsaert, W., 1999: Aspects of Bulk Atmospheric Boundary Layer Similarity under free convective conditions. Rev. Geophy., 37, 439-451.

Caselles, V. and J.A. Sobrino, 1989: Determination of frosts in orange groves from NOAA-9 AVHRR data. Remote Sens. Environ., 29:135-146.

Coll, C. and V. Caselles, 1997: A split window algorithm for land surface temperature from AVHRR data: validation and algorithm comparison. Journal of Geophysical Research, 102(14):16697-16713.

Kustas, W.P., and C.S.T Daughtry, 1989: Estimation of soil heat flux/net radiation ratio from spectral data. Agri. For. Meteorol., 49:205-223.

Massman, W. J., (1999) Molecular diffusivities of Hg vapor in air, O_2 And N_2 near STP and the kinematic viscosity and the thermal diffusivity of air near STP. Atmos. Environ., 33, 453-457.

Monteith, J.L., 1965: Evaporation and environment, Sym. Soc. Exp. Biol., 19, 205-234.

Monteith, J.L., 1973: Principles of Environmental physics. Edward Arnold Press, 241pp.

Palmer, W.C., 1965: Meteorological Drought. Research Paper, No. 45, U.S. Department of Commerce Weather Bureau, Washington, D.C.

Paltridge, G.M. and R.M. Mitchell, 1990: Atmospheric and viewing angle correction of vegetation indices and grass land fuel moisture content derived from NOAA/AVHRR, Remote Sens. Environ. 31:121-135.

Su, Z., J. Wen and L. Wan, 2001: A Methodology for the Retrieval of Land Physical Parameters and Actual Evaporation using NOAA/AVHRR data, paper accepted by the journal of Jilin University press.

Su, Z., and Y. He, 2001: A report for the project: China_CGMS_an information infrastructure for promoting efficient irrigation practices in the North China Plain, BCRS: 4.2/IM-04, pp.19.

Su, Z., and C. Jacobs (Eds.), 2001: Advanced Earth Observation – Land Surface Climate, report USP-2, 01-02, Publications of the National Remote Sensing Board (BCRS), 184pp.

Su, Z., and C. Jacobs (Eds.), 2001b: ENVISAT – Actual Evaporation, report USP-2, 01-05, Publications of the National Remote Sensing Board (BCRS).

Su, Z., and M. Menenti (Eds.), 1999: Mesoscale climate hydrology: the contribution of the new observing systems, Report USP-2, 99-05, Publications of the National Remote Sensing Board (BCRS), 141pp.

Su, Z., 2001: The Surface Energy Balance System (SEBS) for estimation of turbulent heat fluxes at scales ranging from a point to a continent, Hydrol. Earth Sys. Sci. 6(1), 85-99.

Su, Z., M. Menenti, H. Pelgrum, B.J.J.M. Van den Hurk, and W.G.M. Bastiaanssen, 1998: Remote sensing of land surface fluxes for updating numerical weather predictions. In G.J.A. Nieuwenhuis, R.A. Vaughan, and M. Molenaar, (Eds.), Operational Remote Sensing for Sustainable Development. Balkema, 393-402.

Su, Z., T. Schmugge, W.P. Kustas, W.J. Massman, 2001: An evaluation of two models for estimation of the roughness height for heat transfer between the land surface and the atmosphere, J. Appl. Meteor., 40:1933-1951.

Su, Z., G. Roerink, B.H. Gao, Y. Yang, J. Zhang, G. Lu, J.M. Wang, Y.B. He, 2001: Drought monitoring and prediction over continental China - A Perspective approach based on satellite Earth Observation, atmospheric and hydrological modelling, paper presented at the European Geophysical Society's annual meeting, Nice, March 2001.

Valiente, J. A., Nunez, M., Lopez-Baeza, E. and Mereno, J.F. 1995: Narrow-band to broad-band conversion for meteosat-visible channel and broad-band albedo using both AVHRR-1 and –2 channels. Int. J. Remote Sens., 16(6): 1147-1166.

Yan, K., S. Chen, X. Chen, 1997: Depletion Curve Saturation-Excess runoff model, Advances in Water Science 8(1):90-93 (in Chinese).

Yang, Y., J. Qi, L.Wang, 1997: The establishment and application of a meteorological information system for flood and drought prevention, Hydrology, 8(1): 90-93 (in Chinese).

Zhou, G., L. Wang, 1997: Technical report on operational drought monitoring, The proceedings of the meteorological information retrieval, processing and application system, WRIC/MWR (in Chinese).

Zhou, G., Z. Yue, L. Wang, 1998, Estimation of potential evaporation from in-situ meteorology data: research and application, Hydrology, 20-22 (in Chinese).

大范围旱情监测技术

(国家 94.8 技术引进项目)

苏中波

杨　杨

张建云

陆桂华

周国良

儒仁可

戚建国

刘九夫

王　琳

文　军

贾　立

郑　文

岳智慧

陈晓燕

Alterra-rapport 683

Alterra, Green World Research, Wageningen, 2003

目录

前 言

干旱是指在一定区域内近地面生态系统水分不足的一种自然现象，是一种周期性发生的气候现象。产生干旱的直接原因是在较长的时段内降水量偏少，不能满足近地面生态系统水分的需求。

从古至今旱灾都是人类面临的主要自然灾害，即使在科学技术发达的今天，旱灾仍是农业生产及人们生活中最严重的自然灾害。近年来频繁发生的干旱灾害与荒漠化是世界范围内的一个重大环境与气候问题。随着人类社会的经济发展和人口膨胀，水资源短缺现象日趋严重，直接导致了干旱地区的扩大与干旱化程度的加重，干旱问题越来越突出，它直接影响经济社会的可持续发展，并且威胁着人类的生存环境。

我国绝大部分地区属于季风气候区，降水量的季节变化和年际变化非常显著，其空间分布也很不均匀，大范围的干旱在我国频繁发生。据不完全统计，从公元前206年到1949年，2155年内我国共发生较大的旱灾1056起，平均每两年发生一次大旱；1949年以来，我国干旱灾害发生更加频繁，平均年受旱面积为3亿亩以上，因旱灾年均减收粮食约100亿斤。特别是九十年代以来，全国大范围的干旱灾害连年发生，干旱灾害损失也越来越大。干旱已成为我国经济社会可持续发展的一个严重的制约因素。按有关部门预测，本世纪30年代末，我国人口将达16亿，随着人口的大量增加，水资源短缺、干旱和粮食安全等问题会变得动更加突出。因此，开展干旱问题的研究，应用先进的遥感探测技术及水文、气象理论和方法，对大范围的旱情进行监测和预测，减少干旱灾害损失，具有重大的理论意义和应用价值。

水利部水利信息中心根据防汛抗旱业务工作的实际需要，于1996年建立了基于流域水文模型的水文气象干旱监测业务运行系统。该系统将实测地面气象资料和降雨量资料输入流域水文模型计算蒸发能力和土壤含水量，并以土壤缺水量作为干旱程度指标，进行全国旱情分析和监视。该系统是一个在实时降雨和气象要素数据库支持下的自动运行的业务系统，每天给出全国的土壤缺水量分布，多年来较好地指导了抗旱减灾工作。但在应用中感到存在两方面的问题：(1)分辨率低，全国仅以590个雨量站的资料来计算各点的土壤含水量，资料代表性差，不能根据需要及时地反映指定区域的干旱情况；(2)模型计算的是单点资料，全国缺水量分布图是内插绘制的，不能实时客观地反映各流域面上的缺水情况。

近几年，荷兰瓦赫宁恩大学(Wageningen University and Research Centre) Alterra 资源环境研究中心在遥感技术应用方面取得了显著的发展，提出了应用 气象卫星遥感资料进行地表干旱特征参量的反演技术，如反射率、叶面指数、红外辐

射、表面温度、感热和潜热通量、蒸发率、土壤湿度指数等的定量监测方法和技术，并在减少大范围卫星资料处理过程中云对地表观测的影响、相应图像处理应用软件的开发、以及应用微波遥感提取土壤含水量等方面做了大量的研究工作，取得了很好的成果。因此，水利部水利信息中心和荷兰 Alterra 中心在大范围旱情 监测技术方面，从不同的方向均做了大量的研究开发工作，且二者间存在很好的互补性。

在水利部 94.8 项目办公室的大力支持下，作为国外先进技术引进项目于 2000 年 6 月立项。本项目研究开发的主要目标是：研究、引进荷兰 Alterra 资源环境研究中心的地面特征参变量反演及图像处理等遥感应用技术，改进、完善水利部水利信息中心现已应用的全国旱情监视信息系统，更直接、客观、全面、准确地提供旱情信息服务。

项目的执行过程可分为 3 个阶段，各阶段工作内容和取得的成果如下：

第一阶段(2000 年 6 月—2001 年 4 月)：

目的：系统设计及技术准备;取得的主要成果包 括：

(1)资料准备，收集整理了近两年不同季节的气象极轨卫星、同步卫星的图象资料和地面降水、蒸发等观测资料。

(2)第一批中方技术人员(4 人)赴荷工作一周，学习讨论了卫星遥感在旱情监测方面的地面参数反演及图像处理等技术，完成了项目技术方案设计，绘出了系统结构图和数据流程图，制定了技术引进实施方案和工作大纲。

(3)荷方专家于 2001 年 3 月来华讲学，进一步讨论完善了技术设计和实施方案。

第二阶段(2001 年 5 月-2001 年 11 月)：

目的：技术引进、软件移植改造;取得的主要成 果包括：

(1)第二批中方技术人员(4 人)赴荷工作五周，对 SEBS8 程序原程序进行了大规模的改编，将其从小试验区的应用移植到大范围(整个中国)的应用，并适应于自动运行处理模式。此外，通过计算方法的改进，加快了程序的运行计算速度。

(2)根据我国的实际情况及荷方原软件的输入要求，编制了气象卫星原始接收图象的预处理程序。

(3)数据敏感性分析。由于计算方法复杂，参与计算的参数繁多，大范围计算耗时长，对计算机环境要求高。通过对参数进行敏感性分析，确定各参数对计算结果的影响及其敏感性，从而对那些影响不大的参数进行简化计算。

(4)购置和安装图象分析处理软件(ENVI)，并建立应用软件的运行环境。荷兰专家于 2001 年 11 月来华指导工作，开发了部分大气观测资料处理程序，双方完成了应用软件的安装调试，初步完成了软件移植工作。

第三阶段(2001 年 12 月-2002 年 4 月)：

目的：对计算成果进行分析，进一步改进计算方法并进行试验，移植图象时间序列分析软件，编写项目总结报告；取得的主要成果包括：

(1)第三批中方技术人员(5 人)赴荷工作 4 周，完成 2 个月资料的计算计信息提 取，对计算成果进行初步分析。

(2)在分析计算成果的基础上，双方讨论了计算方法的改进和完善。

(3)讨论确定项目技术报告编写提纲和分工，并于 2002 年 4 月完成技术报告的编写工作。

在整个项目的执行过程中，自始至终地得到了水利部水利信息中心、河海大学、及荷兰瓦赫宁恩大学 (Wageningen University and Research Centre) Alterra 资源环境研究中心的大力支持，提供了很好的研究开发环境，是本项目得以顺利完成的基础，在此一并致谢。

《大范围旱情监测技术》项目组

1 概述

1.1 中国的干旱灾害

干旱是一种复杂的自然现象，从不同的应用角度会有不同的理解和认识，没有一个被普遍接受的概念。一般认为，干旱的主要原因是降水量低于平均降水量。降水的不足会有不同的影响，这主要取决于气象条件、生态系统类型、和社会经济环境等其它因子。目前，广泛定义或被普遍接受的干旱类型主要有五种：

（1）以降水指标划分为主的气象干旱，是指一段时间内，降雨量低于平均降雨量；有时也用温度异常和降雨异常相结合来表示。

（2）以土壤水分和作物需水指标划分为主的农业干旱，当植物可利用的降水和土壤持水量低于植物关键生长阶段所需要的水量时，会影响植物的生长，导致牧草或农作物产量的降低。

（3）以地表径流和地下水指标划分为主的水文干旱，一般是由一个或几个因子结合而定义的，如径流量、贮水量和地下水量(位)。

（4）以供水和人类需水指标划分为主的社会经济干旱，是根据获益距平均或希望获益的差距而定义的，它可用社会或经济指标计算。

（5）以地表水分和热量平衡指标划分为主的气候干旱。

中国绝大部分地区属于季风气候区，降水量时空分布很不均匀。年降水量主要集中在汛期的 2-3 个月，汛期降水量可占年降水量的 70% 以 上，特别是在北方地区，年降水量的 80-90%可能集中于 1 至几次降水过 程，而其它时间则是长久的干旱。从全球来看，中国属于降水偏少国家，人均总降水量则更少，仅有 5006m^3，而全球人均平均降水量则为 33975m^3，相比之下，中国只有全球平均的 15%。从水资源的拥有量来看，人均只有 2300m^3，只有世界人均水资源拥有量的 1/4，位居世界第 109 位。每亩的水资源拥有量只有 1900m^3，也只有全球平均水平的 1/4。加之经济飞速发展和城市化，需水量也在不断增加。

此外，中国各地区人均水资源总量差异十分悬殊。比如，经济发达、人口密集的华北地区人均水资源总量最少，只有 500m^3 左右，每公顷平均水资源总量则更少，只有 6750 m^3 左右。西北地区由于人稀 耕地 少，人均、公顷均水资源总量较多，但水资源密度很小，给水资源开发利用带来困难。因此，中国不仅是潜在的极易发生干旱的国家，也是极易受到干旱威胁的国家。

1949 年以来中国较严重的旱灾平均每两年出现一次，平均受旱灾面积达 3.0321×

10^8 亩，占全国各种气候灾害总面积的 59.3%，其中干旱严重的 1959、1960、1961、1978 年的受灾面积均在 5.0×10^8 亩以上，直接粮食损失也在 1.0×10^{10}kg 以上。在所有的自然灾害中，干旱灾害对农业的影响最大。目前，全国灌区农业缺水量约 300 亿 m^3，每年因旱灾减收粮食平均达 100-150 亿 kg。进入 90 年代，每年平均受干旱面积 2400 万 hm^2，比 50 年代增加 1.5 倍以上，受旱成灾面积增加 3 倍。90 年代的前 4 年，因旱灾减收粮食平均每年达 350 亿 kg。目前，全国农村还有 6500 万人和 6000 万头牲畜饮水困难。

2001 年中国遭遇严重旱灾，受旱面积历史最大。全国大部分地区持续干旱，受旱面积已超过 3.5 亿亩，其中旱地 3.3 亿亩，水田 0.2 亿亩。受旱地区主要分布地东北、黄淮大部分和西南部分地区，是进入 90 年代以来受害面积最大的一年，也是连续第三年遭受旱灾。造成旱情的主要原因：一是由于前一年的干旱造成北方地区水利工程蓄水严重不足；再是全国大部分地区降水偏少，抗旱水源也严重不足，5 月初北方八省大型水库蓄水总量比往年同期减少 20%。而北方地区今春多次出现的大风扬沙天气，也使水分蒸发加快，旱情进一步发展。

中国干旱灾害情况大体有以下一些特点：

（1）干旱灾害面积广，分布不均匀

据统计，全国每年农田受旱涝灾害的面积约占总播种面积的 27%左右，而其中 60%左右是旱灾，这说明受旱灾面积是很广的。全国各大区都会有旱灾出现，但分布不均匀，其中黄淮海地区占了全国受旱灾面积的 50%左右，长江中下游也是多旱灾的地区，这两个地区就占了全国受旱灾总面积的 60%以上。

（2）干旱灾害出现频繁，有时持续时间较长

中国幅员辽阔，地形复杂，受季风气候影响，在全国境内，局地性或区域性的干旱灾害几乎每年都会出现。例如，在 1979-1991 年这 13 年 间，其中有 8 年是在华北、东北及华南出现干旱，另有 2 年在长江以南的广大南方地区出现干旱，2 年出现了全国性干旱，1 年为长江流域干旱。在华北地区，在 1951 年-1980 年的三十年中，出现较大范围的干旱 就有 12 年，中等范围的干旱 11 年，其余 7 年出现了范围较小干旱，而这时期长江流域也有 28 年出现了范围不同的干旱。

从干旱持续时间看，许多地区会出现春夏连旱或夏秋连旱，有时甚至春夏秋三季连旱。例如，华北地区干旱的持续时间一般在 1-2 个月或 4-5 个月左右，有些年份干旱持续时间特长，如 1957 年、 1965 年、1968 年、1972 年和 1986 年，长达 5-7 个月，又如

长江流域常会 出现伏旱，但有的年份有的地区会出现连续干旱，例如 1988 年长江流域出现了伏旱，而其中有些地区，如湖南、湖北、上海、江苏、安徽、贵州等省市出现了春夏连旱或夏、伏、秋连旱，持续时间一般在 40 天以上，部分地区达 50-70 天。1994 年 6-8 月江淮地区出现了严重伏旱 ，安徽、江苏、湖北等省伏旱持续时间达 40-50 天，长的达 2 个月以上 ，这一年在全国不少地区还出现了春旱，秋旱范围更广，主要分布在江南、华南、华北和西北东部等地。

（3）干旱常伴随着高温同时出现

许多干旱灾害出现的同时，往往同时出现高温，致使加重旱情，这种情况在长江流域伏旱期更明显，例如 1985 年出现了夏伏连旱，6-8 月份久晴少雨，温度很高，天气燥热，日平均温度都在 30$^{\circ}C$ 以上，鄂西北、鄂东南及三峡河谷地区极端最高温度达 38$^{\circ}C$-40$^{\circ}C$，重庆出现 38$^{\circ}C$ 以上高温天气，其中涪陵、万县高达 40$^{\circ}C$-41$^{\circ}C$。杭州连续 7 天 最高温度达 35$^{\circ}C$-37$^{\circ}C$。气温持续偏高，水分蒸发强烈，助长了伏旱 的发展。1965 年 5-10 月华北地区出现了大旱，这一时期平均气温比常 年偏高 1$^{\circ}C$-2$^{\circ}C$，高温（≥35$^{\circ}C$）日数达 10-35 天，比常年偏多 5-18 天。又如上面已提到的 1994 年江淮流域出现干旱，与此同时，也出现了高温天气，这一地区≥35$^{\circ}C$ 的日数达 20-40 天。

1.2 旱情监测技术及其发展

传统的土壤旱情监测方法主要是根据有限的地面测墒点用称重法或中子仪探测法等测定土壤含水量，这些方法采样速度慢，花费大量人力、物力，代表性差，难以大范围应用，因此多年来国内外科学家一直在探索其他旱情监测的方法和途径并取得了显著成果。美国帕尔默在 1965 年提出一个干旱的定义为“一个持续的、异常的水分缺乏”(Palmer, 1965)。从这个基本思想出发，根据水量平衡原理，考虑蒸 散发、径流和土壤含水量等因素，采用水文计算和水文统计手段，提供了一个能够进行干旱严重程度时空比较的指标并能对地区气候反常现象评价的通用方法，称之为帕尔默指标（PDSI)。在美国它被广泛地应用于描述历史上各年代干旱发生的范围和严重程度，在国际上，帕尔默旱度模式也享有盛名，澳大利亚、加拿大、南非等国家曾先后对 PDSI 方法的适用性作了检验。在我国，中国气象科学研究院安顺清等（1986）将 PDSI 应用于单站干湿气候分析和气候影响评价，河海大学余晓珍（1996）在中国 14 个地区进行了 PDSI 的适用性检验，提出了应用中存在的问题及修正后的帕尔默旱度模式，计算表明 PDSI 可以成为我国这些地区区域干旱分析的有效工具。但 PDSI 计算复杂，一些参

数不易实时收集，在模型框架的建立和水量平衡计算过程中存在着一些假定和任意性，因此一般适用于区域干旱的分析和评定而不适用于实时大范围旱情监测。

我国辽宁水利勘测设计院、四川水文总站、陕西水文总站等单位的科技工作者分别研究提出了当地的农业干旱模型，基本思路考虑了不同农作物生长期间供水与需水的关系，以土壤水量平衡方程表示这种供需与余缺水量，用绝对值或相对比值表示湿润或干旱程度。这种方法有一定的应用价值，但地域性强，数据不易获得，难于实时应用。国家气象中心从气象干旱监测的角度出发将降水量进行统计分析建立雨量分布与旱涝等级和类型的关系，每季度发布全国旱涝级别分布图。由于气象干旱未必与农业干旱相应，同时发布周期长，分辨率低，作用有限。

水利部水利信息中心 1996 年建立了水文气象干旱监测模型，采用实测地面气象资料计算蒸发能力，与实测雨量资料一并输入水文模型，将土壤缺水量作为模型输出并以此作为干旱程度指标的方法监视旱情，建立了自动计算的运行系统并连续运行至今，取得了初步成果，表明了用水文气象资料模型实时监测旱情的可行性。由于没有大范围遥感资料对照订正，同时水文模型没有考虑不同地区地表特征的变化，使输出结果分辨率低并与实际的旱情有很大的偏差，在抗旱决策工作中参考价值不高。用遥感技术监测旱情是近年来国内外研究的热点问题，特别是气象卫星资料具有观测范围大、时间频次高等优点更显示了它的应用优势。国际粮农组织 1997 年开展了用极轨气象卫星 AVHRR 资料对南部非洲进行旱情监视和玉米估产的课题研究。澳大利亚科学家用遥感技术监测作物覆盖、生长状况、土壤湿度，从而辅助干旱范围确定的工作。我国陕西气象局遥感中心利用 AVHRR 资料可见光和近红外通道监测植被指数，用远红外通道亮度温度反演土壤湿度，用这两个参数间接进行干旱动态监测。研究和实际应用结果都表明气象卫星资料是实时监测大范围旱情的有效手段和工具，具有广阔的应用前景。但由于卫星资料反映的是地表对不同电磁波段的反射或辐射特征，并不能直接反映干旱的程度，同时云的存在严重影响观测的结果。

目前，大范围干旱的监测与预测以及干旱决策支持系统也是国际上的研究方向之一。遥感和地理信息系统分别作为大范围内信息获取的有效手段和空间数据的有效管理工具在干旱的监测和预测研究工作中获得了广泛的应用。研究表明，尽管局地的反馈，特别是人类活动所造成的反照率、土壤水分的变化对干旱的发生有着相当的影响，但大范围的持续性干旱主要受制于大尺度的地—气系统的异常反应。 当 今， 国际上对于大范围干旱的监测与预测主要从能量平衡的 角度 出 发，充分利用遥感所获取的下垫面的信息，耦合大气模型和水文模 型，从机理上探讨干旱的发生发展规律，进而对干旱的发生和发展进行监测与预测，建立相应的干旱决策支持系统，达到减灾和防灾目的。

1.3 引进技术的目的和内容

为了建立适用于我国的大范围实时旱情监测系统，本项目引进了荷兰瓦赫宁恩大学(Wageningen University and Research Centre) Alttrra 资源环境研究中心苏中波博士等（Z. Su et al., 1998; Z. Su, 2001, 2002）近年来应用气象卫星资料反演陆面参数的研究成果。其优势是遥感技术可以快速而经济地获取大范围面积内的地表信息，并可以直接监测或间接地反演出大范围干旱所需的非均一地表众多参数和变量，这是利用常规站网监测所无法达到的。土壤含水量是干旱监测与预测的最重要参数之一，而现有的土壤水分计算模型只是简单地将地—气界面的能量和水分分布作为已知变量代入能量平衡方程中来计算土壤的水分分布状况，而能量和水分的空间分布信息实际上难以获取，因而，现有的土壤水分计算模型缺乏实用性。而依靠有限站网监测资料的土壤水分计算模型的计算结果并不十分可靠，因其考虑地表空间变化的不均一性十分有限，故不能依靠现有的水分计算模型来计算土壤的水分空间分布状况，实现干旱监测与预测的目的。由于遥感能提供大范围不均一地表的众多陆面参数值，充分考虑土壤水分分布等的不均一性，因此提高了大范围内土壤水分的监测的实用性。苏中波博士等通过大量研究实验掌握了一整套地表干旱特征参量如反照率、叶面指数、红外辐射、表面温度、感热和潜热通量、蒸发率、土壤湿度指数等的定量监测方法和技术，开发了相应的应用软件，能够及时准确地得到大范围与干旱程度有关的定量数据。

目前的研究成果是在小范围和理想的资料条件下取得的，而实际需要的监测范围和实际的气象卫星资料情况与研究环境相距甚远，难于直接用于旱情监测业务。因此引进这项先进技术，以大范围的卫星遥感资料作为基础，用目前地面高空观测的雨量、温度、湿度、风等水文气象资料与遥感信息和水文模型相结合，研制可实际应用的大范围实时旱情监测模型，进而建立我国实时旱情监测业务系统，逐日输出全国旱情分布图和统计成果，为抗旱决策提供全面可靠的干旱信息，是本项工作的根本目的。

2 原理和方法

2.1 表面能量平衡系统与相对蒸发

表面能量平衡系统（SEBS - Surface Energy Balance System ）是荷兰苏中波研究员等（Z. Su et al., 1998; Z. Su, 2001, 2002）近期开发的应用卫星对地观测的可见光、近红外和热红外波段资料，结合实测气象数据或大气模式输出数据，根据表面能量平衡原理估算不同尺度的地表大气湍流通量，从而估算地表相对蒸发的方法。

热红外遥感为表面温度的函数，是对表面能量平衡状态的瞬时观测。表面能量平衡是由表面净辐射驱动的，白天主要是太阳短波辐射。在地表，净辐射在感热通量、潜热通量和地面热通量间平衡，任一时刻的地表能量平衡如下：

$$R_n = G_o + H + \lambda E \tag{2.1}$$

其中，R_n是净辐射量，G_0是土壤热通量，H是感热通量，为地表变热的能量，λ是水的汽化热，表示一定体积的水通过蒸散发从液态变为气态所需的能量，E为水蒸散通量，λE是潜热通量。

净辐射计算公式为：

$$\begin{aligned} R_n &= K^{\downarrow} - K^{\uparrow} + L^{\downarrow} - L^{\uparrow} \\ &= (1-\alpha)R_{sw} + \varepsilon(\varepsilon'\sigma T_a^4 - \sigma T_0^4) \end{aligned} \tag{2.2}$$

其中，$K^{\downarrow}, K^{\uparrow}, L^{\downarrow}, L^{\uparrow}$分别为向下、向上的短波辐射和向下、向上的长波辐射，α为反照率，R_{sw}为向下的太阳辐射，σ为斯蒂芬-波尔兹曼常数，ε为地表比辐射率，ε'为大气比辐射率，T_a为气温，T_0为地表温度。

土壤热通量计算公式为：

$$G_o = R_n.[\Gamma_c + (1-f_c).(\Gamma_s - \Gamma_c)] \tag{2.3}$$

其中，Γ_c=0.05 为植被覆盖区 (Monteith, 1973)，Γ_s=0.315 为裸土区 (Kustas, 1989)，f_c为植被覆盖比率。

$R_n - G_0$即感热和潜热通量之合为地表有效能量，决定地表观测温度的关键是有效能量中感热通量和潜热通量各是多少，这是由可利用的水量通过蒸散作用从地表转移到大气的过程控制的，因此通过对地表温度的计算即可得到地表的潜热通量λE和实际蒸发E。

相对蒸发为实际蒸发和蒸发能力之比。实际蒸发一方面取决于气象条件（温度、风力、太阳辐射、湿度等）决定的蒸发能力，另一方面取决于土壤含水量，因此相对蒸发很好地反映了土壤的相对干湿程度。应用遥感资料和气象观测数据相结合估算相对蒸发，将其与实测资料对比即能够确定土壤干旱程度。

2.2 表面能量平衡系统估算相对蒸发的方法

表面能量平衡系统估算相对蒸发主要包括 4 部分内容：确定地表物理参数；摩擦风速、感热通量和稳定度长度计算；确定动量和热量传输粗糙度；相对蒸发估算。

2.2.1 地表物理参数确定

系统所需要的地表物理参数有太阳辐射、反照率、植被指数、地表比辐射率、地表温度等。

太阳辐射：

$$R_{sw} = I_{sc} \cdot e_0 \cdot \cos\theta_z \cdot \exp(-m \cdot \tau) \tag{2.4}$$

其中，I_{sc} 为太阳常数，e_0 为轨道偏离校正数，θ_z 为太阳天顶角，m 为大气质量，τ 为光学厚度。

反照率(Valiente et al., 1995)：

$$\alpha = 0.545 \cdot r_1 + 0.320 \cdot r_2 + 0.035 \tag{2.5}$$

其中，r_1，r_2 分别为气象卫星 NOAA/AVHRR 第一、二通道的反射率，由卫星的测量值经双向反射校正后得到。

植被指数：

$$NDVI = \frac{r_2 - r_1}{r_2 + r_1} \tag{2.6}$$

地表比辐射率(Caselles and Sobrino 1989)：

$$\varepsilon = \varepsilon_v f_c + \varepsilon_g (1 - f_c) + 4 < d\varepsilon > f_c (1 - f_c) \tag{2.7}$$

式中 $f_c = \dfrac{NDVI - NDVI_{\min}}{NDVI_{\max} - NDVI_{\min}}$，为植被覆盖比率，$< d\varepsilon >$ 为非线性参数，取值为 0.002。

ε_v 和 ε_g 分别为 10.5-12.5 微米光谱区间表面植被覆盖区和裸土区的比辐射率，

$\varepsilon_v = 0.985 \pm 0.007$，$\varepsilon_g = 0.960 \pm 0.010$。

地表温度(Coll and Caselles, 1997)：

$$T_0 = T_4 + \left[1.34 + 0.39 \times (T_4 - T_5)\right] \times (T_4 - T_5) + 0.56 + \alpha \times (1 - \varepsilon) - \beta \times \Delta\varepsilon$$

$$\alpha = W^3 - 8W^2 + 17W + 40 \qquad 2.8)$$

$$\beta = 150 \times (1 - W/4.5) \quad (\text{W: g/cm}^2)$$

其中，T_4、T_5为 NOAA/AVHRR 第 4 和第 5 通道的亮度温度，W 为大气水汽含量，$\Delta\varepsilon$ 为第 4 和第 5 通道的比辐射率差。

2.2.2 总体大气相似理论确定摩擦风速、感热通量和稳定度长度

感热通量需应用总体大气传输相似理论求出。在大气的地表边界层，平均风速和平均温度廓线的相似关系一般写为如下积分式：

$$u = \frac{u_*}{k}\left[\ln\left(\frac{z-d_0}{z_{0m}}\right) - \Psi_m\left(\frac{z-d_0}{L}\right) + \Psi_m\left(\frac{z_{0m}}{L}\right)\right] \qquad (2.9)$$

$$\theta_0 - \theta_a = \frac{H}{ku_*\rho C_p}\left[\ln\left(\frac{z-d_0}{z_{0h}}\right) - \Psi_h\left(\frac{z-d_0}{L}\right) + \Psi_h\left(\frac{z_{0h}}{L}\right)\right] \qquad (2.10)$$

其中，u_*为摩擦风速，ρ为空气密度，k为卡门常数，C_p为定压比热，z为高度，d_0为位移高度，z_{0m}为动量传输粗糙度，θ_0为地表位温，θ_a 为边界层高度位温，z_{0h}为热量传输粗糙度，ψ_m和ψ_h分别为动量和热量传输莫宁-奥勃霍夫稳定度校正函数，L为稳定度长度，定义为：

$$L = -\frac{\rho C_p u_*^3 \theta_v}{kgH} \qquad (2.11)$$

其中，g为重力加速度，θ_v为近地面虚位温。

用迭代方法解(2.9)-(2.11)式构成的非线性方程组，即可得到摩擦风速 u_*，稳定度长度L和感热通量H。

2.2.3 动量和热量传输粗糙度确定

上述方程组中，动量和热量传输粗糙度这两个重要的参数必须提前确定。在有详细地表资料的情况下一般采用参数化方法，但在大范围应用并且地表资料不充分时确定参数就

有一定的困难。在 SEBS 系统中建立了应用遥感资料计算动量和热量传输粗糙度模型，解决了这两个参数的设定问题。

根据地表粗糙度与植被指数间的关系，动量传输粗糙度按下式计算(Su, 2001)：

$$Z_{0m} = 0.0005 + 0.5 \times \left(\frac{NDVI}{NDVI_{\max}} \right)^{2.5} \tag{2.12}$$

相应地，平面位移高度 $d_0 = Z_{0m} \times 4.9$，植被高度 $h = Z_{0m} / 0.136$。

热量传输粗糙度从下式得到：$Z_{0h} = Z_{0m} / \exp(kB^{-1})$

这里 B^{-1} 为无量纲热量传输系数，kB^{-1} 计算模型如下(Su et al. 2001)：

$$kB^{-1} = \frac{kC_d}{4C_t \frac{u_*}{u(h)} \left(1 - e^{-n/2}\right)} f_c^2 + \frac{k \cdot u_* / u(h) \cdot z_{0m} / h}{C_t^*} f_c^2 f_s^2 + kB_s^{-1} f_s^2 \tag{2.13}$$

式中 f_c 和 f_s 分别为植被和裸土的覆盖比率，C_d 为植物拖曳系数，取值为 0.2，C_t 为叶面热量传输系数，取值为 0.01，$u(h)$ 为作物冠层顶的水平风速，裸土热量传输系数 $C_t^* = \mathrm{Pr}^{-2/3} \mathrm{Re}_*^{-1/2}$，其中 $\mathrm{Pr} = 0.71$，为普朗特数，粗糙度雷诺数 $\mathrm{Re}_* = h_s u_* / \nu$，$h_s$ 为裸土粗糙度高度，空气运动粘滞数 $\nu = 1.37 \cdot 10^{-5} (p_0 / p)(T / T_0)^{1.81}$ (Massman, 1999)，P 和 T 为环境气压和气温，$P_0 = 101.3kPa$，$T_0 = 273.15K$。裸土 kB_s^{-1} 以下式计算(Brutsaert, 1982)：

$$kB_s^{-1} = 2.46 \left(\mathrm{Re}_* \right)^{1/4} - \ln[7.4] \tag{2.14}$$

在（2.13）中，n 为作物冠层内风廓线消光系数，是冠层累积叶面拖曳区域的函数，以下式表达(Su et al., 2001)：

$$n = \frac{C_d \cdot LAI}{2u_*^2 / u(h)^2} \tag{2.15}$$

式中 $LAI = \left[NDVI \times \frac{1 + NDVI}{1.000001 - NDVI} \right]^{0.5}$，为叶面指数。

2.2.4 表面能量平衡极端状态方法估算相对蒸发

感热通量得到后，理论上通过（2.1）式即可估算出潜热通量。然而由于计算是应用观测的风速、温度等数据进行的，因此观测数据的不确定性会对感热通量的估算结果带来较大的误差，同样也影响到潜热通量的估算。为此在 SEBS 中，根据能量平衡在两种极端状态下的感热通量特征，通过对感热通量在最干状态和最湿状态的计算将估算误差限制在一定范围内，从而提高计算结果的可靠性。

在最干状态时，由于土壤湿度的原因使潜热通量或蒸散发为零，从而感热通量达到最大值。根据（2.1）式可知：

$$\lambda E_{dry} = R_n - G_0 - H_{dry} \equiv 0，或者$$

$$H_{dry} = R_n - G_0 \tag{2.16}$$

而在最湿状态，蒸发能力即为蒸发量，也就是取决于地表大气条件的有效能量。这时的感热通量达到最小值，即

$\lambda E_{wet} = R_n - G_0 - H_{wet}$，*或者*

$$H_{wet} = R_n - G_0 - \lambda E_{wet} \tag{2.17}$$

相对蒸发如下表达：

$$\Lambda_r = \frac{\lambda E}{\lambda E_{wet}} = 1 - \frac{\lambda E_{wet} - \lambda E}{\lambda E_{wet}} \tag{2.18}$$

将（2.1），(2.16）和（2.17）代入（2.18）式，经代数运算可得：

$$\Lambda_r = 1 - \frac{H - H_{wet}}{H_{dry} - H_{wet}} \tag{2.19}$$

同时定义干燥度指数 DSI（Drought Severity Index）：

$$DSI = 1 - \Lambda_r = \frac{H - H_{wet}}{H_{dry} - H_{wet}} \tag{2.20}$$

感热通量H的值以H_{dry}和H_{wet}为上下限，上限H_{dry}从（2.16）式得到，下限H_{wet}则需要将（2.17）式与彭曼-默特斯联合方程（Monteith, 1965)相结合求出。联合方程写为：

$$\lambda E = \frac{\Delta \cdot r_e \cdot (R_n - G_0) + \rho C_p \cdot (e_{sat} - e)}{r_e \cdot (\gamma + \Delta) + \gamma \cdot r_i} \qquad (2.21)$$

式中e和e_{sat}分别为实际水气压和饱和水气压，γ为干湿表常数，Δ为饱和水气压随温度的变化率，r_i为总体地表内部阻力，r_e为外部或空气动力阻力。直接计算潜热通量λE的困难在于内部阻力r_i取决于有效土壤水分，而其大小难于预先得到，因而在此避免直接用r_i计算λE。

在最湿状态下，根据定义内部阻力$r_i \equiv 0$，应用（2.21）式，最湿状态下感热通量为：

$$H_{wet} = \left((R_n - G_0) - \frac{\rho C_p}{r_{ew}} \cdot \frac{e_s - e}{\gamma} \right) \Big/ \left(1 + \frac{\Delta}{\gamma} \right) \qquad (2.22)$$

式中，最湿状态下外部阻力为：

$$r_{ew} = \frac{1}{k u_*} \left[\ln\left(\frac{z - d_0}{z_{0h}} \right) - \psi_h \left(\frac{z - d_0}{L_w} \right) + \psi_h \left(\frac{z_{0h}}{L_w} \right) \right] \qquad (2.23)$$

最湿状态下稳定度长度为：

$$L_w = -\frac{\rho u_*^3}{kg \cdot 0.61 \cdot (R_n - G_0) / \lambda} \qquad (2.24)$$

H_{wet}确定后，相对蒸发Λ_r和潜热通量λE即随之确定。

3 资料处理和实际计算

3.1 资料需求分析

根据项目要求，应用 SEBS 系统实现大范围干旱实时监测需要取得对地面大范围的动态监测资料，能够从中提取计算相对蒸发所需要的各项参数，同时对有些变量要进行参数化设置。

NOAA/AVHRR 为美国极地轨道气象卫星，每天对同一地区进行 4 次观测，观测时间大致为 2 时、8 时、14 时和 20 时。分辨率为 1.1 公里，具有可见光、近红外、中红外和两个热红外 5 个光谱通道，能够从中提取反照率、地面温度、植被指数、地表比辐射率等物理参数。另外计算中需要的气温、水气压、风速等资料需要从地面气象观测资料中提取。表 2.1 为计算中需要的变量及其来源，表明需要准备如下资料：

1. 遥感资料：NOAA/AVHRR 第 1, 2, 4, 5 通道数据；
2. 地面观测资料: 海平面气压, 气温, 露点温度, 风速, 水平能见度；
3. 其他资料：测站高程, 观测时间等。

表 2.1 SEBS 输入变量及来源

符号（单位）	变量或参数	来源或设置
$\alpha(-)$	反照率	AVHRR 1, 2 通道
$NDVI(-)$	植被指数	AVHRR 1, 2 通道
$\varepsilon(-)$	地表比辐射率	NDVI
$\varepsilon'(-)$	大气比辐射率	$9.26\times10^{-6}\times T_a^2$
$f_c(-)$	植被覆盖率	NDVI
$LAI(-)$	叶面指数	NDVI
$z(m)$	边界层高度	1000
$d_0(m)$	平面位移高度	$z_{0m}\times4.9$
$z_{0m}(m)$	动量粗糙度	NDVI
$z_{0h}(m)$	热量粗糙度	模型计算
$u(ms^{-1})$	边界层风速	地面观测风速
$u(h)(ms^{-1})$	作物冠层顶风速	u, d_0, z_{0m}
$T_0(^0K)$	地表温度	AVHRR 4, 5 通道
$T_a(^0K)$	边界层温度	地面观测气温
$p_a(pa)$	边界层气压	地面海平面气压，测站高度
$e_s(pa)$	饱和水气压	T_0, T_a
$e(pa)$	实际水气压	地面气温、露点，p_a
$\tau(-)$	大气光学厚度	地面观测能见度
$\theta_a(^0K)$	边界层位温	T_a，p_a，海平面气压
$\theta_0(^0K)$	地表位温	T_0，p_a，海平面气压
$\theta_v(^0K)$	地表虚位温	θ_0，地面露点
$R_{sw}(Wm^{-2})$	太阳辐射	年、月、日、时

3.2 资料选取和预处理

本项目的研究目的是为了建立我国大范围旱情实时监测业务系统，因此选取计算资料时主要考虑以下要求：第一，足够长（两个月）的连续时间；第二，足够大的范围；第三，卫星观测时间和地面观测时间基本同步。

为此，选取了 2000 年 7 月、8 月逐日 14 时前后的 AVHRR 第 2 轨资料，覆盖范围以我国中部地区为主，宽度为 2000 公里左右。同时选取了逐日 14 时我国近 600 个气象站的地面观测资料。

资料预处理分为 2 部分：卫星资料预处理和气象资料预处理。

3.2.1 卫星资料预处理

1，应用 ENVI 软件对 AVHRR 1B 数据进行如下两项处理：

（1）数据定标：应用 Calibrate Data 功能将 1, 2 通道数据校正为反射率, 将 3, 4, 5 通道数据校正为开氏温度。

（2）数据定位：应用 Build Geometry File 功能对卫星图象各象素进 行位置和太阳, 卫星的高度角计算，产生各个象素点的经纬度文件和太 阳, 卫星高度角文件。

2，将 1, 2 通道数据进行双向反射校正：

卫星可见光通道收到的总体辐射量 I^s 可分为 5 个部分：

$$I^s = I^{dir} + I^{sca} + I^{sky} + I^{ind} + I^{mul} \tag{3.1}$$

其中，I^{dir} 为地面直接反射的太阳光，I^{sca} 为大气中分子和粒子的单向散射，I^{sky} 为地面反射的天空单向散射中撞击地面部分，I^{ind} 为地面反射辐射后来散射至卫星部分，I^{mul} 为分子多级重复散射的贡献。双向反射校正公式为(Paltridge and Mitchell, 1990)：

$$r = \frac{K(1-M) - \sec\phi_s \sum_{j=0}^{1} \Phi_j Q_j(m)}{4\cos\theta \cdot g(m) e^{-m\tau}(1+m\tau)} \tag{3.2}$$

其中，K 为卫星测量值，θ、ϕ_s 分别为太阳高度角和卫星高度角，M 为分子多重散射，$Q(.)$ 为总体源函数，$g(.)$ 为空气质量 m 的相关函数（m 为太阳到地面再到卫星的空气总质量），τ 为气溶胶光学厚度（由地面观测的能见度资料推算），$\Phi(.)$ 为分子和气溶胶散射的散射相函数。

3.2.2 气象观测资料预处理

气象资料在计算应用前要进行数据插值,数据转换两项预处理工作。

1， 数据插值

进行大范围计算必须使用大量气象地面观测站的实际观测资料，并且要将点观测资料通过数据插值计算形成与卫星图象一致的气象要素图象。在本项目中采用了距离加权平均方法，根据卫星图象的经纬度文件将计算需要的各气象要素插值到卫星图象相应的每一个象素上。

2，数据转换

根据表 2.1 可知，在计算中应用的气象要素大部分不是直接使用观测数据，而是由观测数据转换而来，因此气象数据的转换是一项重要的预处理工作。下面为气象数据的转换方案：

$$\text{地面气压：}\ P_s = P_0\left(1-\frac{alt}{44331}\right)^{(1/0.1903)} \quad (Pa) \qquad (3.3)$$

其中，P_0 为测站海平面气压，alt 为测站高度。

$$\text{饱和水气压：}\ e_s = 611\exp\left(\frac{17.502\times T_a}{240.97+T_a}\right) \quad (Pa) \qquad (3.4)$$

式中，T_a 为地面测站观测气温。

$$\text{实际水气压：}\ e = 611\exp\left(\frac{17.502\times Tdewpt}{240.97+Tdewpt}\right) \quad (Pa) \qquad (3.5)$$

式中，$Tdewpt$ 为地面测站观测露点温度。

$$\text{比湿：}\ q = (R_d/R_v)\times e/P_s \quad (Kg/Kg) \qquad (3.6)$$

式中，R_d，R_v 分别为干空气和水汽的比气体常数。

近地面位温：$\theta_a = T_a\left(\frac{P_s}{P_0}\right)^{-0.286} \quad (K)$ （3.7）

近地面虚位温：$\theta_v = T_a \times (1+0.61\times q)\times\left(\frac{P_s}{P_0}\right)^{-0.286} \quad (K)$ （3.8）

3.3 计算过程和成果

3.3.1 参数设定

在 SEBS 的应用中首先对计算涉及的大量参数进行取值设定，这些参数中一部分为物理常数，另一部分则是通过试验取得的经验数据。表 3.1 为系统计算参数设定表。

表 3.1 SEBS 参数设定表

符号（单位）	参数	设置值
$I_{sc}(Wm^{-2})$	太阳常数	1367.0
$W(g/cm^2)$	大气水汽含量	1.92
$\Delta\varepsilon(-)$	4, 5 通道比辐射率差	0.002
$\varepsilon_v(-)$	植被区比辐射率	0.98
$\varepsilon_s(-)$	裸土区比辐射率	0.95
$z(m)$	边界层高度	1000.
$\gamma(PaK^{-1})$	干湿表常数	67.
$R_v(Jkg^{-1}K^{-1})$	水汽比气体常数	461.5
$R_d(Jkg^{-1}K^{-1})$	干空气比气体常数	287.04
$C_p(Jkg^{-1}K^{-1})$	定压比热	1005.
$\lambda(Jkg^{-1})$	水的蒸发（凝结）潜热	2.43×10^{6}
$g(ms^{-2})$	重力加速度	9.8
$\sigma(Wm^{-2}K^{-4})$	斯蒂芬-波尔兹曼常数	5.678×10^{-8}
$k(-)$	卡门常数	0.41

3.3.2 计算流程

SEBS 系统计算程序用 IDL 语言编写，在 ENVI 软件环境下应用。计算过程分为预处理、地表物理参数计算和 SEBS 相对蒸发计算 3 部分，共 8 个过程。图 3.1 为计算流程图。

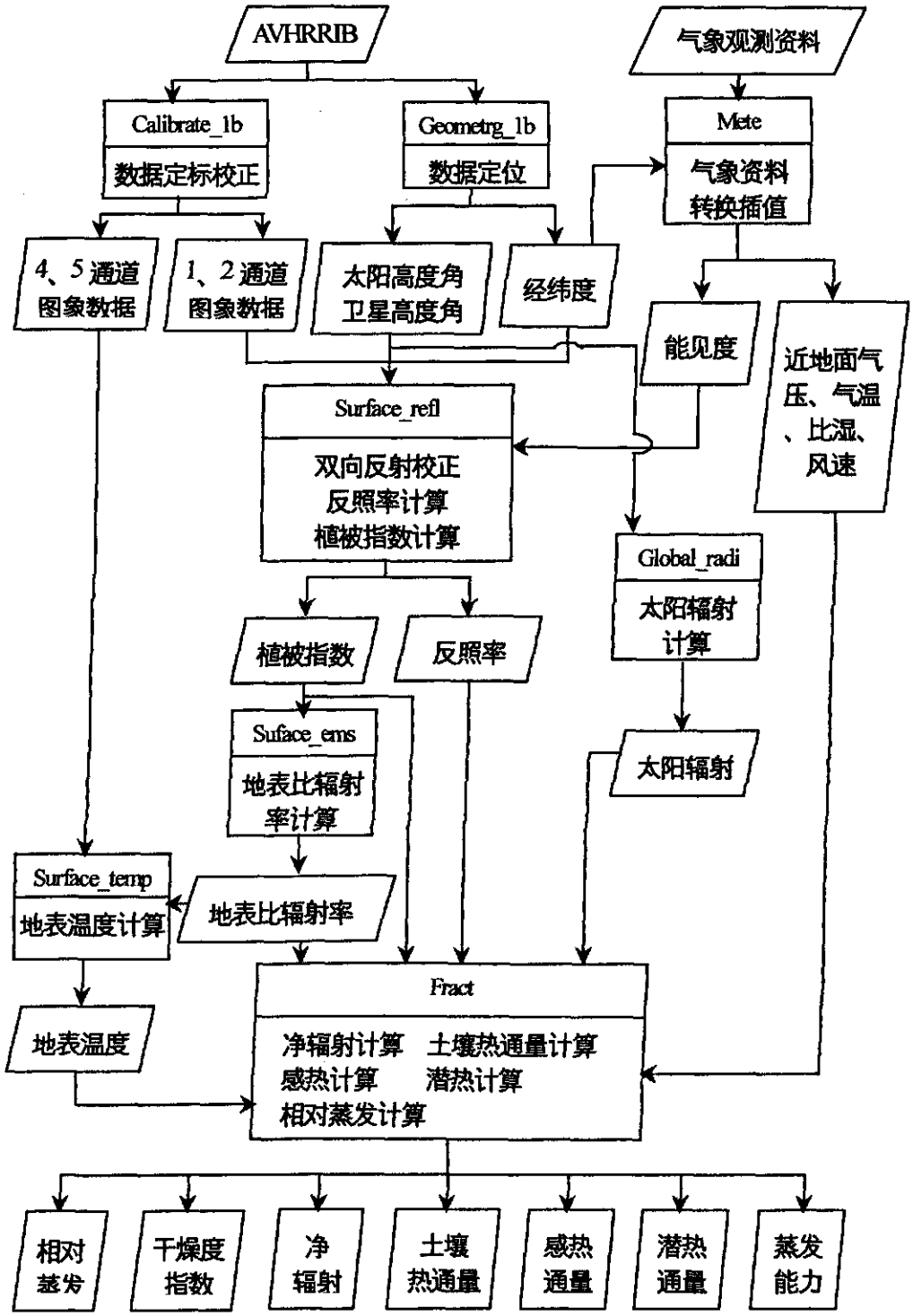

图 3.1. SEBS 计算流程

3.3.3 计算成果

SEBS 计算成果以图象文件形式输出，为如下 12 项(表 3.2)：

表 3.2 SEBS SEBS 计算成果

序号	文件名	内容
1	Relative_evaporation	相对蒸发
2	Drought_severity_index(DSI)	干燥度指数
3	Net_radiation	净辐射
4	Soil_heat_flux	土壤热通量
5	Sensible_heat_flux	感热通量
6	Latent_heat_flux	潜热通量
7	Potential_evaporation	蒸发能力
8	Global_radiation	太阳辐射
9	Broad_band_albedo	反照率
10	Emissivity	地表比辐射率
11	NDVI	植被指数
12	Land_surf_temp	地表温度

4. 成果检验分析

4.1 检验分析方法

由于 SEBS 输出成果内容丰富，同时计算范围大，时间长，难于取得与计算成果相应的大量实测数据，因此本项目仅对最直接反映干旱状况的相对蒸发数据进行成果分析。

为了考察 SEBS 在业务中应用的能力，同时考虑将 SEBS 与目前的应用系统相结合建立实用的我国大范围旱情实时监测业务系统，本项目采用将 SEBS 成果与水利部水利信息中心目前运行的土壤缺水量旱情监测成果对比分析的方式进行成果检验。

4.1.1 土壤缺水量监测方法简介

该方法为水利部水利信息中心研制，主要内容为应用实时水文气象资料与水文模型相结合计算全国范围土壤缺水量，并根据各地土壤缺水量与干旱程度的关系确定干旱等级，实现大范围旱情的连续监测。自 1996 年建立计算模型以来，应用实时气象资料以逐日迭代的方式计算并输出多种水文气象旱情监测成果，在国家防汛抗旱水文气象信息处理应用业务中已连续运行 6 年，具有一定的监测效果，表明了用水文气象资料和模型实时监测旱情的可行性。但由于没有大范围遥感资料对照订正，同时水文模型没有考虑不同地区地表特征的变化，使输出结果分辨率低，与实际的旱情也有不小偏差。

此方法分为两个部分，第一，蒸发能力计算；第二，土壤缺水量计算。蒸发能力计算采用休正的彭曼公式，根据应用要求，用实时天气资料中气温、风速、湿度及云量等要素估算全国约 600 个测点的逐日蒸发能力，将估算成果制成全国日蒸发能力分布图作为应用产品向户 提供，详见周国良等(1998)“利用实时气象资料估算蒸发能力的研究 与应用”一文。土壤缺水量计算是将上述各天气测站的日蒸发能力估算值与同一测站的日雨量数据输入消退曲线超渗产流模型（详见颜开等(1997)，“消退曲线超渗产流模型”），逐日实时估算全国各地的 理想土壤缺水状况。这里所称的“理想土壤”，是指在无灌溉条件下，纯天然、无植被、大范围、对该地区有代表性的裸土土壤。根据历史资料分析确定不同土壤干旱的缺水指标，从而评定各地理想土壤的干旱程度。

4.1.2 检验方式

将 2000 年 7、8 两月每天约 600 站的土壤缺水量数据提出，根据测站的经纬度将 SEBS 计算成果相对蒸发的图象数据中相应点的数据取出形成表格数据文件，将两种计算结果进行相关分析。

4.2 检验分析结果

4.2.1 综合分析

选取 27—41° N、105-126° E 范围内（含边界）的气象基本站该时 段 24 天 NOAA 卫星观测图象的计算结果进行分析，平均每天有 69.5 站其计算值在[0，1.05]区间内，按站数统计，约占有计算结果的 48.5%，占该区域总站数的 31.9%，其余部分要么是卫星观测通道未覆盖区域，或者是计算结果超出范围——包括完全有云覆盖地区和有薄云被误判区 域。

4.2.2 相关分析

用计算的相对蒸发，与地面气象站对应，从图上按经纬度最接近点提取其对应点的值，与气象站观测计算的土壤缺水量进行相关分析。图 4.1 给出植被根部土壤含水量和干旱指数的关系。其中 R^2 是一个统计相关参数，它表示趋势线预报值与实际观测值的逼近程度，1 表示预报值完全逼近实际观测值，0 表示不逼近。以下结果通过了线性相关检验，负相关表明干湿的对应关系正确。但是，按区域分别统计，东部平原区的相关程度较中部要差。

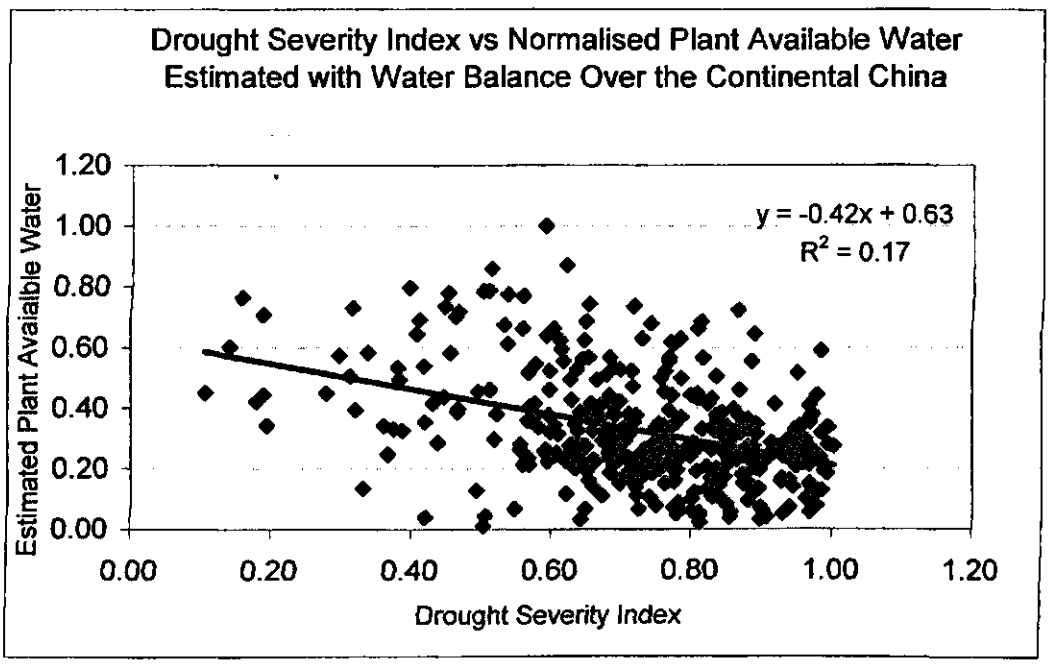

图 4.1 地面观测站的归一化的植被根部土壤含水量和干旱指数的关系

4.2.3 个例分析

4.2.3.1 单站逐日分析

从时间方面比较分析，结果不太理想，部分站甚至出现微弱的正相关，可见逐日的可比性不强。随机抽查部分有资料日数较多的测站统计逐日的变化趋势，下图给出几个地面观测站植被根部土壤含水量和干旱指数的关系，可见其反相变化的特点。说明干旱指数能有效地反映植被根部土壤含水量的实际情况。

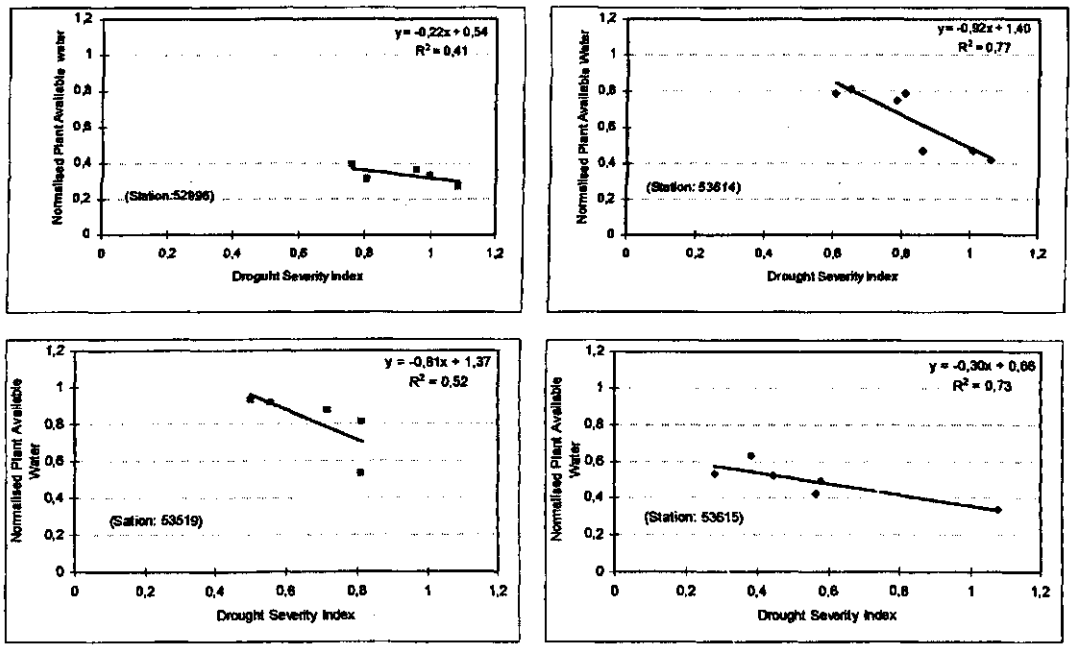

图 4.2 几个地面观测站归一化的植被根部土壤含水量和干旱指数的关系

4.2.3.2 单日面上分析

为便于从空间分析比较，挑选某日云覆盖区域较小，有效数据较多的。以 2000 年 7 月 8 日统计，线性相关系数为 0.59265，n=117。为了比较不同方法得到的结果对干旱程度的响应，图 4.3 分别给出能量平衡方法得到的全国蒸发比、水文气象干旱和土壤缺水量在不同日期分布图。可以看出三种参数有一定的可比性，基本的空间分布趋势也比较一致。由於蒸发比基於卫星遥感观测，在有云覆盖时不能很好地反映地面的真实情况，但在无云覆盖情况下的计算结果有真实的物理意义。

4.2.4 典型对比分析

仍以 7 月 8 日为例，从水利部水利信息中心以前的干旱监视业务系统中水文气象干旱分布图上，选取以平原为主的干湿对比区域各一个，进行对比分析。

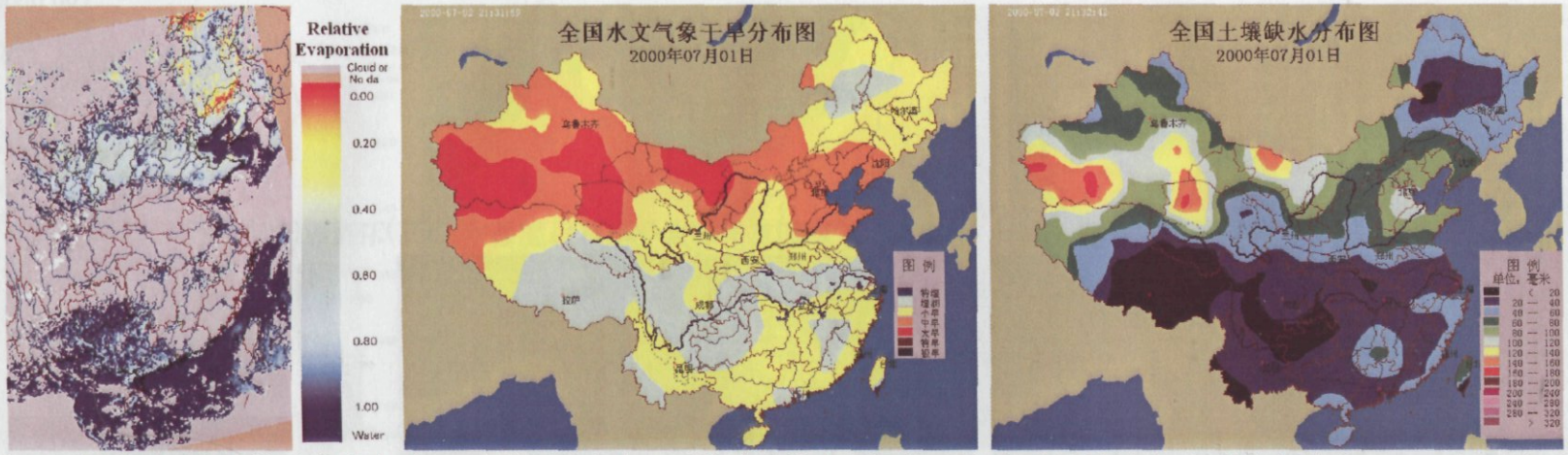

图 4.3a. 用能量平衡计算的蒸发比(左)、水资源信息中心系统计算的水文气象干旱(中)和土壤缺水(右)的全国分布，2000 年 7 月 1 日

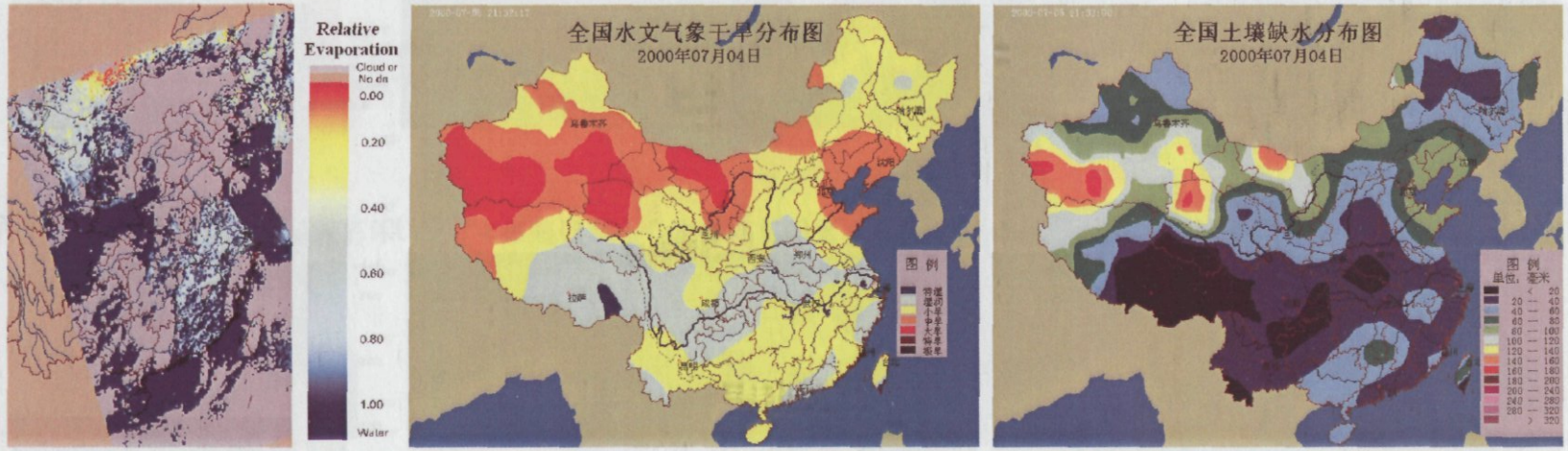

图 4.3b. 用能量平衡计算的蒸发比(左)、水资源信息中心系统计算的水文气象干旱(中)和土壤缺水(右)的全国分布，2000 年 7 月 4 日

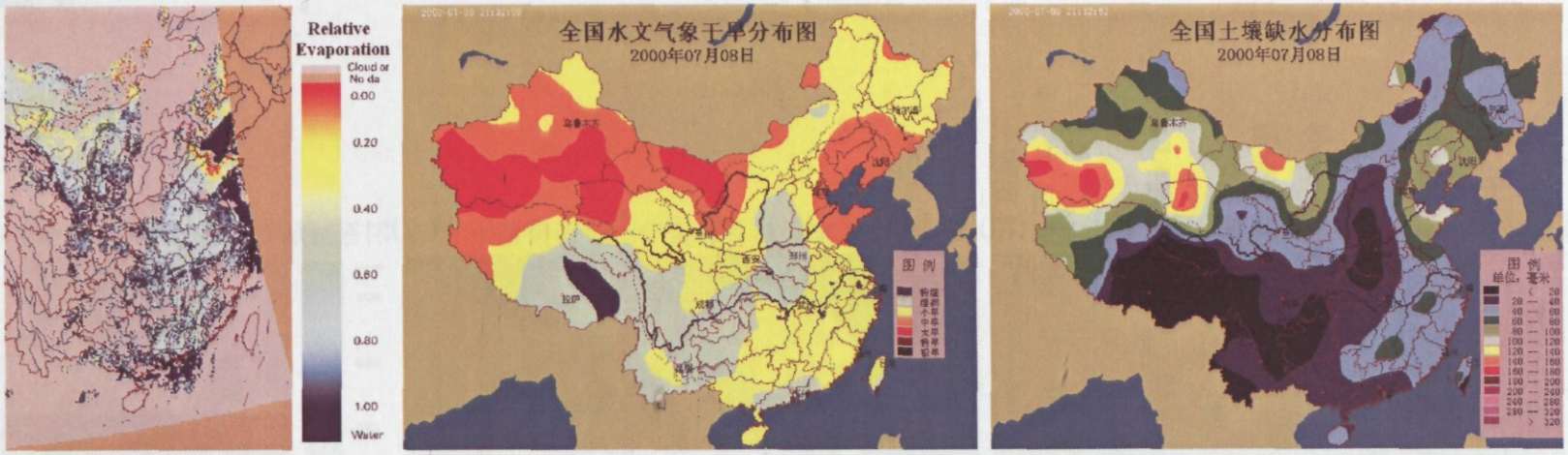

图 4.3c. 用能量平衡计算的蒸发比(左)、水资源信息中心系统计算的水文气象干旱(中)和土壤缺水(右)的全国分布，2000 年 7 月 8 日

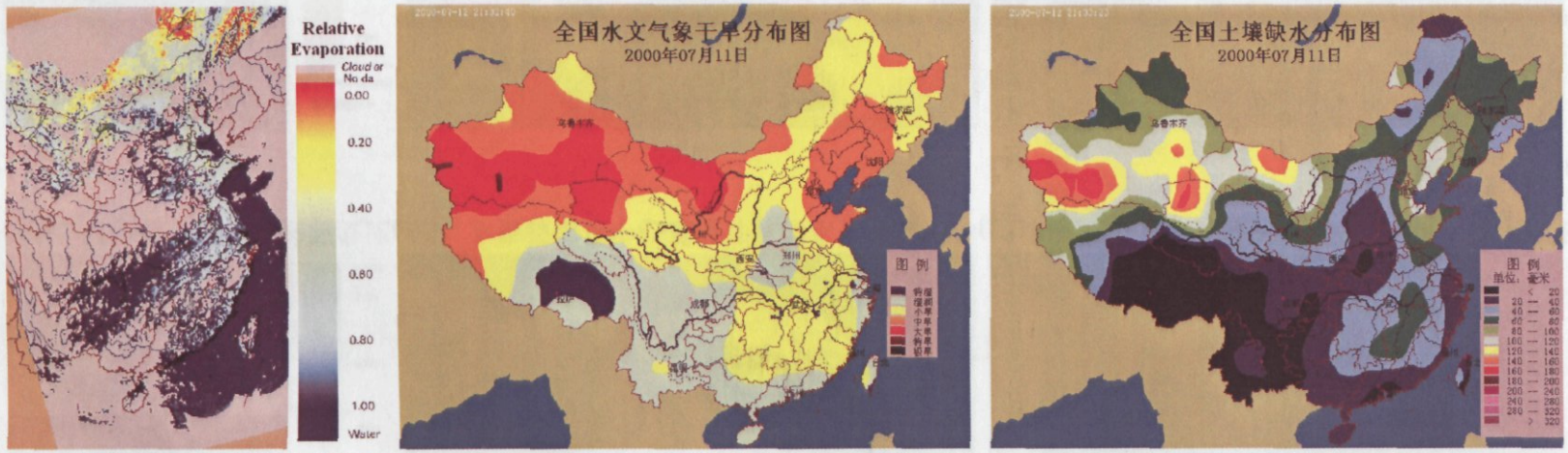

图 4.3d. 用能量平衡计算的蒸发比(左)、水资源信息中心系统计算的水文气象干旱(中)和土壤缺水(右)的全国分布，2000 年 7 月 11 日

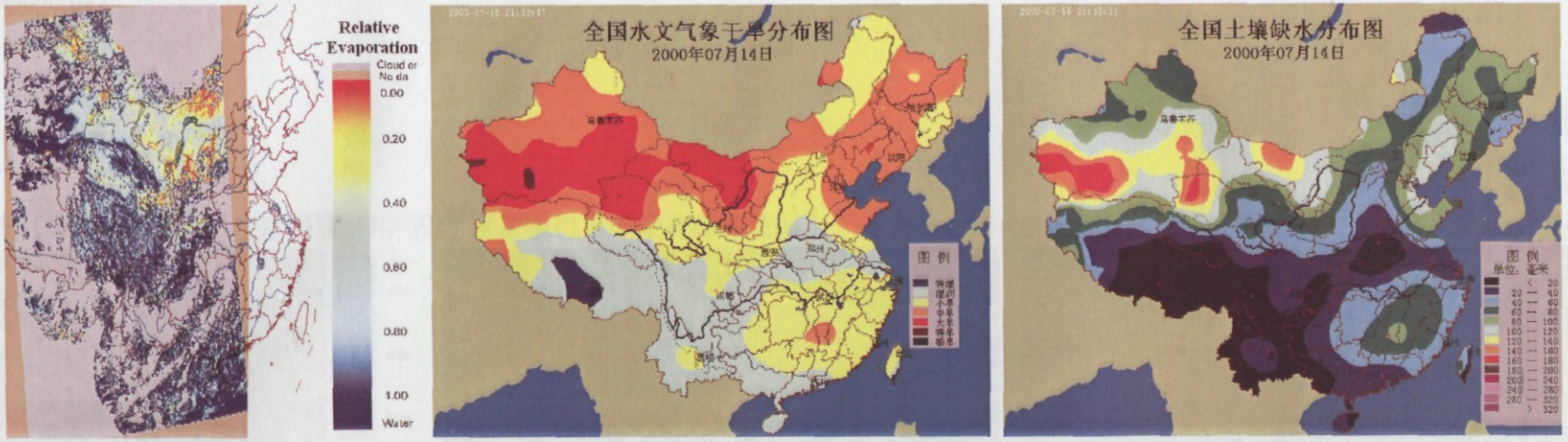

图 4.3e. 用能量平衡计算的蒸发比(左)、水资源信息中心系统计算的水文气象干旱(中)和土壤缺水(右)的全国分布，2000 年 7 月 14 日

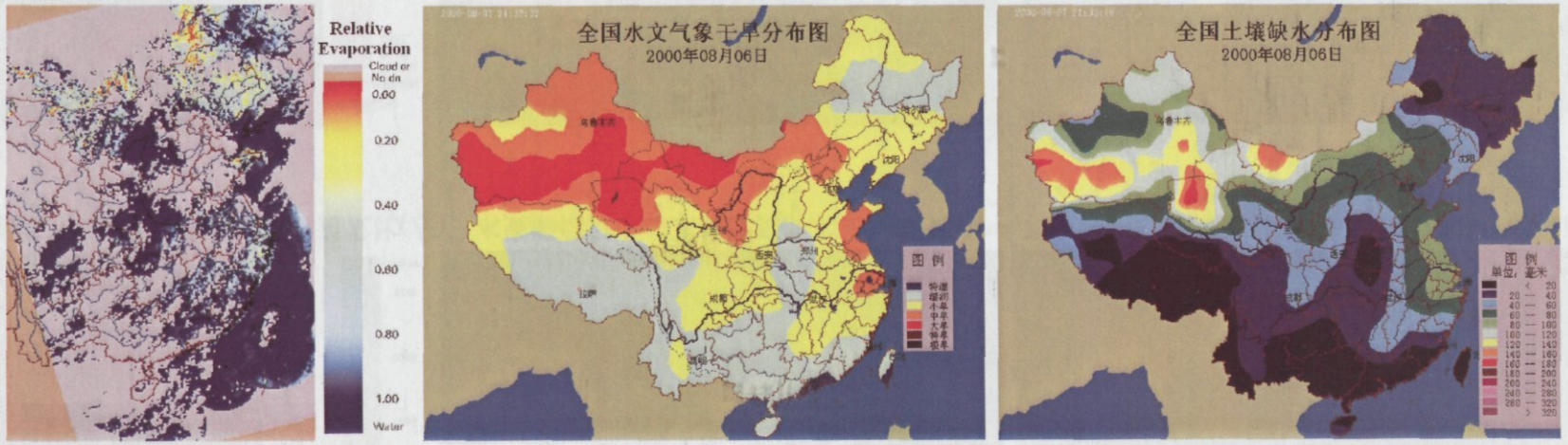

图 4.3f, 用能量平衡计算的蒸发比(左)、水资源信息中心系统计算的水文气象干旱(中)和土壤缺水(右)的全国分布，2000 年 8 月 6 日

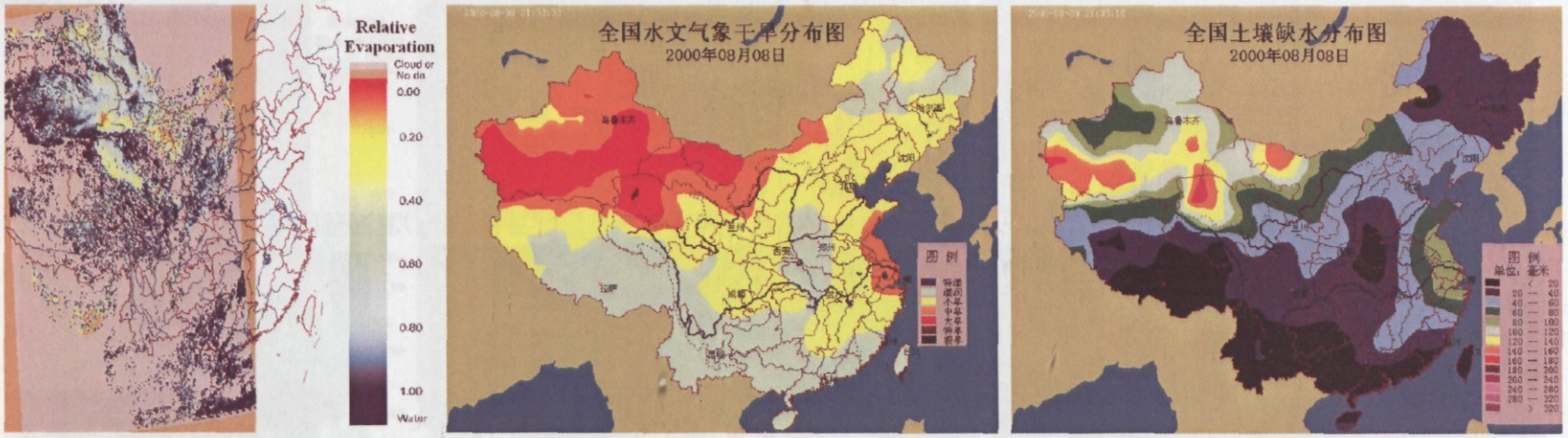

图 4.3g. 用能量平衡计算的蒸发比(左)、水资源信息中心系统计算的水文气象干旱(中)和土壤缺水(右)的全国分布，2000 年 8 月 8 日

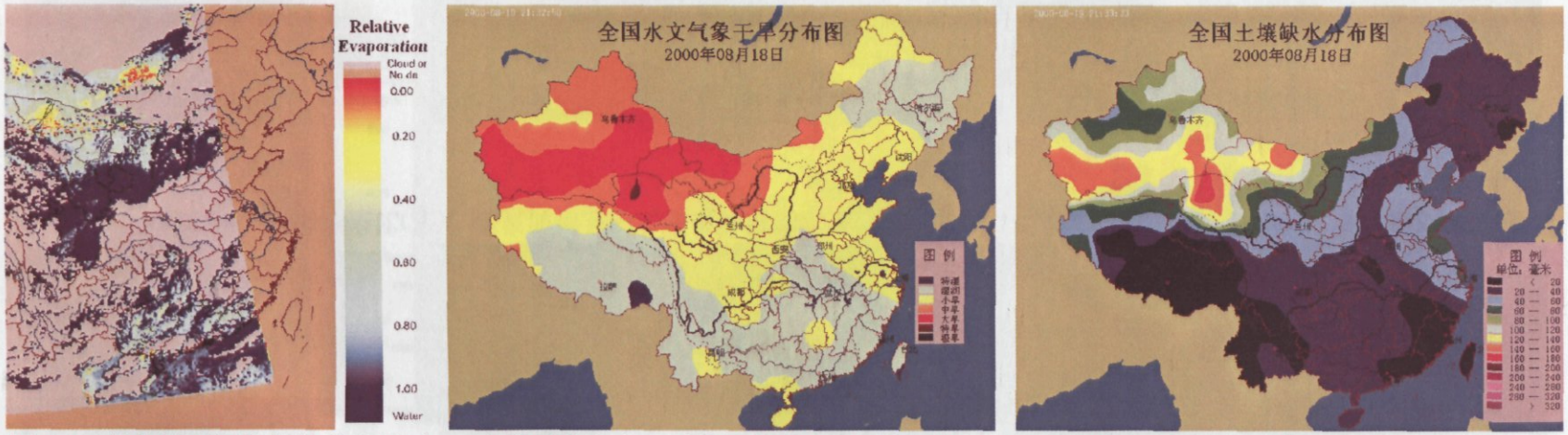

图 4.3h, 用能量平衡计算的蒸发比(左)、水资源信息中心系统计算的水文气象干旱(中)和土壤缺水(右)的全国分布，2000 年 8 月 18 日

干区范围为：35—41° N、116—122° E，有 20 个有效测站；湿区范围为：30—37° N、110—116° E，有 21 个有效测站。

统计干湿区的平均相对蒸发计算值，分别为 0.41166 和 0.7798，对应的平均土壤缺水量分别为 98.35%和 28.77%。干湿的对应关系与物理意义相符，差异明显，计算结果很好。下图分别给出华北和华东地区植被根部土壤有效含水量和干旱指数的统计关系。尽管 R 平方值不是很高，但根部含水量与干旱指数的反相位关系很明显。

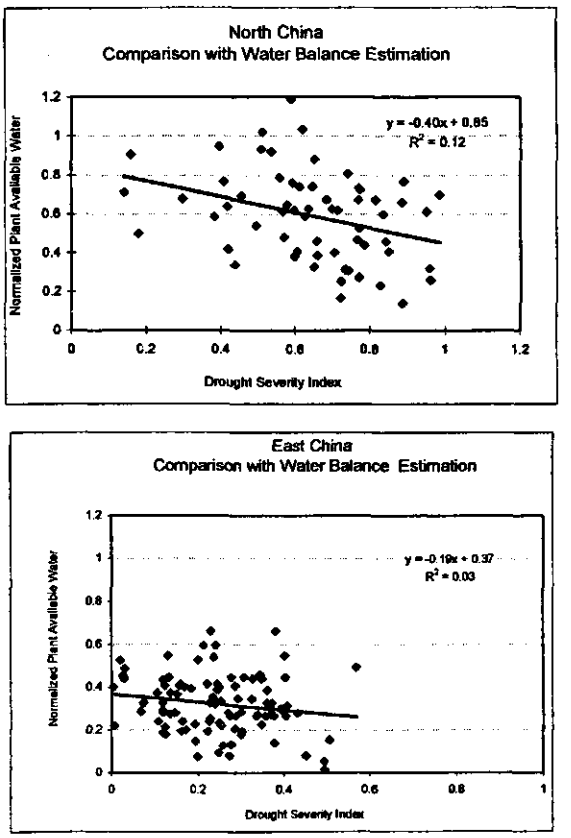

图 4. 4. 华北和华东地区植被根部土壤含水量和干旱指数的统计关系

4.3 误差成因分析

上面分析可见，从空间分布和时间演变两个方面来看，计算结果还有不尽人意处。误差产生的原因可能有如下几个方面：

（1）卫星观测资料的订正处理不够。在对卫星资料的预处理中主要进行了可见光通道的双向反射订正，但对各通道的大气订正没有深入进行。对计算中涉及的气溶胶、水汽等参数采用了经验数据，而这些参数正是影响大气透明度的主要因子。每天大气状况的不同使卫星观测的资料在反演地面参数时出现误差。

（2）供对比分析使用的测站土壤缺水量，由于是用气象观测资料和水文模型计算

后得到的，本身就存在一定的误差，空间可比性也存在问题。

（3）计算环节较多，同时计算将遥感数据和气象观测数据相结合进行，在卫星图象反演和测站观测数据空间化的过程中都存在误差，因此总体误差还不小。

（4）少量资料的代用也值得商榷，可能也是误差的重要原因。

4.4 问题讨论

（1）相对蒸发计算结果出现一些 0 值点，按理说应是极端干旱才对，实际上不完全是。由于感热通量的计算独立于表面能量平衡方程，因而有可能出现计算的感热通量大于总有效能量的不合理结果，在这种情况下也将相对蒸发处理为 0 值。这种情况表明感热通量的计算还存在一定的问题，需要进一步探讨。

（2）检验分析表明，计算结果离实际应用还有很大差距。首先由于云雾覆盖和大气透明度等因素的影响，逐日计算数据的可用范围平均不到整个计算范围的一半，其次，各日连续观测的可比性还不够，即从时间上看，每日的观测值之间可能存在系统偏差。估计上述误差分析的第一点是造成这种现象的主要原因。另外，计算成果与目前实际应用的土壤缺水量数据比较的相关程度还不十分令人满意。加强资料预处理、与土壤缺水量计算相结合并加入时间序列的资料分析和数据差补等将是今后的改进方向。

5. 结语

为实现我国大范围旱情的动态监测，本项目引进了荷兰先进的气象卫星反演有关地面物理参数的方法，以及遥感数据和地面观测数据相结合的表面能量平衡系统计算相对蒸发的技术。由于气象卫星监测范围大、频次高，资料易于获取，同时这项技术的物理意义明确，可操作性强，因此具有较高的实用价值。在引进的过程中对原来的技术方法进行了改进，将小范围实验性的工作扩展为大范围业务性的应用。实际成果表明引进和改造工作取得了初步成功，反映出这项技术对大范围旱情实时动态监测的可行性，但同时也表明目前的结果还不能达到实时旱情监测业务应用的要求。在下一步的成果转化和推广应用工作中，将对引进技术进行深入分析研究并加以改造，在此基础上将计算结果通过与其他旱情监测方法的成果同化、结合的方式，建立适合我国应用的大范围旱情实时监测系统并投入业务应用。

参考文献

Brutsaert, W. 1982. Evaporation into the atmosphere, Reidel, Dordrecht, 299 pp.

Brutsaert, W., 1998: Land-surface water vapor and sensible heat flux: Spatial variability, homogeneity, and measurement scales. Water Resour. Res., 34, 2433-2442.

Brutsaert, W., 1999, Aspects of Bulk Atmospheric Boundary Layer Similarity under free convective conditions. Rev. Geophy., 37, 439-451.

Caselles, V. and J.A. Sobrino, 1989, Determination of frosts in orange groves from NOAA-9 AVHRR data. Remote Sens. Environ., 29:135-146.

Coll, C. and V. Caselles, 1997, A split window algorithm for land surface temperature from AVHRR data: validation and algorithm comparison. Journal of Geophysical Research, vol. 102, 14:16697-16713.

Kustas, W.P., and C.S.T Daughtry, 1989c, Estimation of soil heat flux/net radiation ratio from spectral data. Agri. For. Meteorol., 49,205-223.

Massman, W. J., (1999) Molecular diffusivities of Hg vapor in air, O_2 And N_2 near STP and the kinematic viscosity and the thermal diffusivity of air near STP. Atmos. Environ., **33,** 453-457.

Monteith, J.L., 1965: Evaporation and environment, Sym. Soc. Exp. Biol., 19, 205-234.

Monteith, J.L., 1973, Principles of Environmental physics. Edward Arnold Press, 241pp.

Palmer, W.C., 1965. Meteorological Drought. Research Paper No. 45, U.S. Department of Commerce Weather Bureau, Washington, D.C.

Paltridge, G.M. and R.M. Mitchell, 1990, Atmospheric and viewing angle correction of vegetation indices and grass land fuel moisture content derived from NOAA/AVHRR, Remote Sens. Environ. 31:121-135.

Su, Z., J. Wen and L. Wan, 2001, A Methodology for the Retrieval of Land Physical Parameters and Actual Evaporation using NOAA/AVHRR data, paper accepted by the journal of Jilin University press.

Su, Z, and Y. He, 2001, A report for the project: China_CGMS_an information infrastructure for promoting efficient irrigation practices in the North China Plain, BCRS: 4.2/IM-04, pp.19.

Su, Z., and C. Jacobs (Eds.), 2001a: Advanced Earth Observation – Land Surface Climate, report USP-2, 01-02, Publications of the National Remote Sensing Board (BCRS), 184pp.

Su, Z., and C. Jacobs (Eds.), 2001b: ENVISAT – Actual Evaporation, report USP-2, 01-05, Publications of the National Remote Sensing Board (BCRS).

Su, Z., and M. Menenti (Eds.), 1999: Mesoscale climate hydrology: the contribution of the new observing systems, Report USP-2, 99-05, Publications of the National Remote Sensing Board (BCRS), 141pp.

Su, Z., 2001: The Surface Energy Balance System (SEBS) for estimation of turbulent heat fluxes at scales ranging from a point to a continent, Hydrol. Earth Sys. Sci. 6(1), 85-99.

Su, Z., M. Menenti, H. Pelgrum, B.J.J.M. Van den Hurk, and W.G.M. Bastiaanssen, 1998: Remote sensing of land surface fluxes for updating numerical weather predictions. In G.J.A. Nieuwenhuis, R.A. Vaughan, and M. Molenaar, (Eds.), Operational Remote Sensing for Sustainable Development. Balkema, 393-402.

Su, Z., T. Schmugge, W.P. Kustas, W.J. Massman, 2001: An evaluation of two models for estimation of the roughness height for heat transfer between the land surface and the atmosphere, J. Appl. Meteor.,40,1933-1951.

Su, Z., G. Roerink, B.H. Gao, Y. Yang, J. Zhang, G. Lu, J.M. Wang, Y.B. He, 2001: Drought monitoring and prediction over continental China - A Perspective approach based on satellite Earth Observation, atmospheric and hydrological modelling, paper presented at the European Geophysical Society's annual meeting, Nice, March 2001.

Valiente, J. A., Nunez, M., Lopez-Baeza, E. and Mereno, J.F., 1995: Narrow-band to broad-band conversion for meteosat-visible channel and broad-band albedo using both AVHRR-1 and –2 channels. Int. J. Remote Sens. 16(6): 1147-1166.

颜开, 陈树娥, 陈信华.消退曲线超渗产流模型[J].1997, 水科学进展, Vol.8, No.1, 90-93.

杨扬, 戚建国, 王琳. 防汛抗旱雨情气象信息系统的建设和应用[J]. 水文, 1998 年增刊, 58-61

周国良, 王琳. 实时旱情监视技术报告. 雨情气象信息接收处理应用系统技术 报告文集. 1997. 水利部水利信息中心.

周国良, 岳智慧, 王琳. 利用实时气象资料估算蒸发能力的研究与应用[J]. 水文, 1998 年增刊, 20-22